The Plant Cell, Vol. 32: 2979–2996, September 2020, www.plantcell.org © 2020 ASPB.

The Cyclin CYCA3;4 Is a Postprophase Target of the APC/C^{CCS52A2} E3-Ligase Controlling Formative Cell Divisions in Arabidopsis

Alex Willems, Jefri Heyman, Thomas Eekhout, Ignacio Achon, Jose Antonio Pedroza-Garcia, Tingting Zhu, Lei Li, Ilse Vercauteren, Hilde Van den Daele, Brigitte van de Cotte, Ive De Smet, and Lieven De Veylder[1]

Department of Plant Biotechnology and Bioinformatics, Ghent University, Ghent B-9052, Belgium
Center for Plant Systems Biology, VIB, Ghent B-9052, Belgium

ORCID IDs: 0000-0002-7211-8388 (A.W.); 0000-0003-3266-4189 (J.H.); 0000-0002-2878-1553 (T.E.); 0000-0002-4553-1257 (I.A.); 0000-0001-8258-0157 (J.A.P.-G.); 0000-0002-0904-7636 (T.Z.); 0000-0002-1820-9852 (L.L.); 0000-0001-9561-8468 (I.V.); 0000-0002-4271-6694 (H.V.d.D.); 0000-0001-7236-9243 (B.v.d.C.); 0000-0003-4607-8893 (I.D.S.); 0000-0003-1150-4426 (L.D.V.)

The anaphase promoting complex/cyclosome (APC/C) controls unidirectional progression through the cell cycle by marking key cell cycle proteins for proteasomal turnover. Its activity is temporally regulated by the docking of different activating subunits, known in plants as CELL DIVISION PROTEIN20 (CDC20) and CELL CYCLE SWITCH52 (CCS52). Despite the importance of the APC/C during cell proliferation, the number of identified targets in the plant cell cycle is limited. Here, we used the growth and meristem phenotypes of Arabidopsis (*Arabidopsis thaliana*) CCS52A2-deficient plants in a suppressor mutagenesis screen to identify APC/C^{CCS52A2} substrates or regulators, resulting in the identification of a mutant cyclin *CYCA3;4* allele. CYCA3;4 deficiency partially rescues the *ccs52a2-1* phenotypes, whereas increased CYCA3;4 levels enhance the scored *ccs52a2-1* phenotypes. Furthermore, whereas the CYCA3;4 protein is promptly broken down after prophase in wild-type plants, it remains present in later stages of mitosis in *ccs52a2-1* mutant plants, marking it as a putative APC/C^{CCS52A2} substrate. Strikingly, increased CYCA3;4 levels result in aberrant root meristem and stomatal divisions, mimicking phenotypes of plants with reduced RETINOBLASTOMA-RELATED PROTEIN1 (RBR1) activity. Correspondingly, RBR1 hyperphosphorylation was observed in CYCA3;4 gain-of-function plants. Our data thus demonstrate that an inability to timely destroy CYCA3;4 contributes to disorganized formative divisions, possibly in part caused by the inactivation of RBR1.

INTRODUCTION

Cell division represents an essential biological process, not only allowing the transfer of genetic information from one generation to the next, but also permitting multicellular organisms to grow and develop. The latter implies that cell proliferation must be controlled in such a way that a building plan can be executed. When a new cell arises through cell proliferation from the stem cells, it frequently undergoes a number of cell divisions that are eventually followed by the implementation of a cell cycle exit program. Both the proliferative activity of the stem cells and the timing of cell cycle exit need to be strictly regulated, as perturbations in either impair growth (De Veylder et al., 2007; Polyn et al., 2015; Shimotohno and Scheres, 2019). One of the key players that controls both events is the anaphase promoting complex/cyclosome (APC/C; see Heyman and De Veylder [2012] for an extensive review on the plant APC/C). The APC/C is a conserved E3 ubiquitin ligase that provides unidirectional transit through the cell cycle by targeting key cell cycle proteins for degradation by the 26S proteasome (Marrocco et al., 2010). The plant APC/C consists of at least 11 core subunits, of which most are encoded by single-copy genes that are essential for plant viability (Page and Hieter, 1999; Capron et al., 2003; Van Leene et al., 2010; Heyman and De Veylder, 2012). Its structural backbone consists of the tetratricopeptide repeat interaction domain-containing proteins APC6, APC7, APC8, and APC3 (the latter being present in two copies in Arabidopsis [*Arabidopsis thaliana*]: APC3a/CDC27 and APC3b/HOBBIT) and is completed by APC1, APC4, and APC5. Together, these proteins correctly position the catalytic subunits APC2 and APC11, which perform the ubiquitin transfer reaction, the coactivator APC10, and one activator subunit belonging to one of two classes, respectively called CELL DIVISION CYCLE20 (CDC20) or CDC20 HOMOLOG1 (CDH1), the latter also known in plants as CELL CYCLE SWITCH52 (CCS52; Tarayre et al., 2004; Kevei et al., 2011; Heyman and De Veylder, 2012). The activator proteins recruit the APC/C ubiquitination targets through recognition of conserved amino acid motifs such as the Destruction box (D-box; Pfleger and Kirschner, 2000; De Veylder et al., 2007; da Fonseca et al., 2011).

The plant *CCS52* gene was first identified in *Medicago*, where it plays an important role in establishing the polyploid tissues of the root nodules (Cebolla et al., 1999). The described link between *CCS52* expression, initiation of differentiation, and the onset of the endocycle was later confirmed in other plant species. For example, in tomato (*Solanum lycopersicum*), decreased *CCS52A* levels were found to cause a reduction in endoreplication and fruit size, whereas in rice (*Oryza sativa*), mutation of *CCS52A* resulted in dwarf growth and problems with kernel development due to

[1] Address correspondence to lieven.deveylder@psb.vib-ugent.be.
The author responsible for distribution of materials integral to the findings presented in this article in accordance with the policy described in the Instructions for Authors (www.plantcell.org) is: Lieven De Veylder (lieven.deveylder@psb.vib-ugent.be).
www.plantcell.org/cgi/doi/10.1105/tpc.20.00208

IN A NUTSHELL

Background: Cell division in multicellular organisms is strictly regulated so that tissues of the body form correctly. One way to achieve such regulation is the selective breakdown of rate-limiting cell division proteins when they are no longer needed. The Anaphase-Promoting Complex/Cyclosome (APC/C) is a key player in this process, marking cell cycle proteins for destruction through attachment of a ubiquitin group. The APC/C recognizes its targets with the help of an activator subunit, such as the CELL CYCLE SWITCH 52 A2 (CCS52A2) protein. Mutant Arabidopsis plants lacking CCS52A2 display dwarfism, due to severe disorganization of the cell division patterns in the root and shoot.

Question: We aimed to identify which cell cycle regulators are marked for breakdown by the CCS52A2-activated APC/C to explain why plants struggle to grow when appropriate APC/C activation cannot occur. As the dwarf growth phenotype might be explained by the inappropriate accumulation of an APC/C target protein, we searched in the *ccs52a2* mutant background for secondary mutations that restored plant growth.

Findings: A mutation preventing the production of the CYCLIN A3;4 (CYCA3;4) cell cycle regulator partially counteracted the dwarf growth phenotype of *ccs52a2* mutant plants. The lack of the closely related *CYCA3;1* and *CYCA3;2* genes did not restore mutant dwarf growth, highlighting the unique role of CYCA3;4. We confirmed that CYCA3;4 is a true target for APC/$C^{CCS52A2}$-mediated breakdown, as it remained present throughout mitosis in the *ccs52a2* mutant, but disappeared after prophase in wild-type plants. Moreover, CYCA3;4 plays a unique role in the cell divisions that relate to stem cells, possibly through phosphorylating the key cell cycle regulator Retinoblastoma-related 1 (RBR1). Combined, the data indicate that CCS52A2-activated APC/C controls stem cell-associated cell divisions through the temporal control of CYCA3;4 levels, marking CYCA3;4 as an important regulator in the field of stem cell biology.

Next steps: The lack of CYCA3;4 does not completely restore *ccs52a2* mutant growth, meaning that additional proteins need to be timely marked for destruction by CCS52A2-activated APC/C. Identifying and characterizing these targets and studying their interplay with CYCA3;4 will clarify how timely and spatial controls of cell division controls plant growth.

a reduction of endoreplication in the endosperm (Mathieu-Rivet et al., 2010; Su'udi et al., 2012; Xu et al., 2012).

In Arabidopsis, three isoforms of CCS52 are present, two A types (CCS52A1 and CCS52A2) and one plant-specific B type (CCS52B; Tarayre et al., 2004; Kevei et al., 2011). Prophase-confined expression of *CCS52B* indicates that it might play a role in the degradation of M-phase proteins necessary for the progression of mitosis (Yang et al., 2017). By contrast, *CCS52A1* and *CCS52A2* are thought to repress cell division in a tissue-specific manner that is determined by their expression pattern. Within the root, *CCS52A1* is predominantly expressed at the root elongation zone where it controls cell cycle exit, illustrated by an increased root meristem size in *ccs52a1* knockout plants (Vanstraelen et al., 2009). Additionally, *CCS52A1* is expressed in leaves and trichomes, where it controls the number of endocycles (Lammens et al., 2008; Boudolf et al., 2009; Larson-Rabin et al., 2009; Baloban et al., 2013; Heyman et al., 2017). Along with controlling endocycle progression in the leaf, CCS52A2 appears to be important for maintaining the low proliferation status of the quiescent center (QC) and the organizing center of respectively the root and the shoot, as *ccs52a2-1* mutant plants show a severe disruption of meristem organization, leading to a short root, dwarf growth, and a strong reduction in the development of reproductive organs (Vanstraelen et al., 2009; Liu et al., 2012).

Currently, only a relatively limited set of proteins have been thoroughly characterized as targets of the CCS52-activated APC/C. In Arabidopsis, protein stability of the A-type cyclin CYCA2;3 was found to be reduced by APC/$C^{CCS52A1}$ to control the onset of endoreduplication (Boudolf et al., 2009). The ETHYLENE RESPONSE FACTOR115 (ERF115) transcription factor was initially identified as an interactor of CCS52A2 in a tandem affinity purification experiment and was shown to be an important rate-limiting factor of QC cell division (Heyman et al., 2013). Another protein identified as a CCS52A2 target is CELLULOSE SYNTHASE-LIKE D5 (CSLD5), a cell wall biosynthesis enzyme that plays a role in the assembly of the newly forming cell plate during division and that is rapidly degraded upon completion of mitosis, but not in the *ccs52a2-1* mutant background (Gu et al., 2016). In rice, targets of the CCS52 homolog TILLER ENHANCER (TE)/TILLERING AND DWARF (TAD1) include the GRAS-family transcription factor MONOCULM1 (MOC1), which is involved in shoot branching and tillering (Lin et al., 2012; Xu et al., 2012), several members of the PYR/PYL/RCAR family of abscisic acid receptors (Lin et al., 2015), and the homolog of stem cell regulator SHORT ROOT (SHR; Lin et al., 2020).

Here, we have utilized an ethyl methanesulfonate (EMS) suppressor screen to identify novel APC/$C^{CCS52A2}$ targets, based on the growth-inhibitory phenotype of *ccs52a2-1* knockout plants. We show that one of the identified revertants encodes a mutant allele of *CYCA3;4* and demonstrate this cyclin to be a specific target of APC/$C^{CCS52A2}$ that ensures correct stem cell organization.

RESULTS

Identification of *pkn2* as a *ccs52a2-1* Suppressor Mutant

Compared to wild-type (Columbia-0 [Col-0]) plants, *ccs52a2-1* mutant seedlings display a short root phenotype (Figures 1A and 1B; Supplemental Figures 1A and 1B; Vanstraelen et al., 2009; Heyman et al., 2013). This phenotype was used to screen for

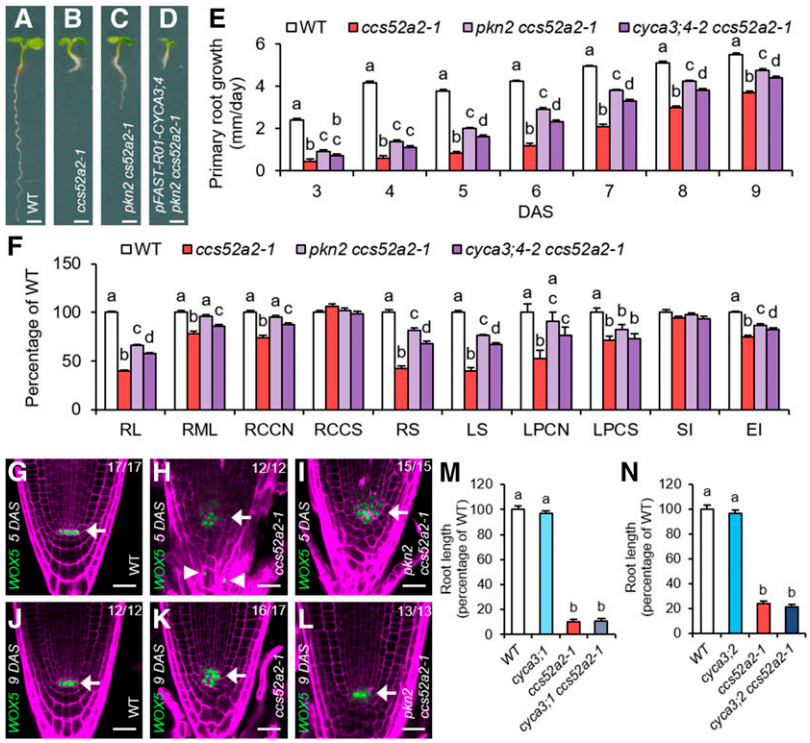

Figure 1. The *pkn2* Mutation Partially Rescues the *ccs52a2-1* Phenotypes.

(A) to **(D)** Representative seedlings of the wild type (WT) **(A)**, *ccs52a2-1* **(B)**, and *pkn2 ccs52a2-1* without **(C)** and with **(D)** the *pFAST-R01-CYCA3;4* complementation construct at 5 DAS. Scale bars represent 1 mm.

(E) and **(F)** Growth characteristics of the wild type (WT), *ccs52a2-1*, and the double mutants *pkn2 ccs52a2-1* and *cyca3;4-2 ccs52a2-1*. **(E)** Primary root growth from 3 to 9 DAS ($n \geq 62$). **(F)** Phenotypes of the primary root at 9 DAS and the shoot and the first leaf pair at 21 DAS. RL, Root length ($n \geq 62$); RML, root meristem length ($n \geq 25$); RCCN, root cortical cell number ($n \geq 25$); RCCS, root cortical cell size ($n \geq 25$); RS, rosette size ($n \geq 56$); LS, leaf size ($n \geq 31$); LPCN, leaf pavement cell number ($n = 15$); LPCS, leaf pavement cell size ($n = 15$); SI, stomatal index ($n = 15$); EI, endoreplication index ($n \geq 15$). Bars represent estimated marginal means, and error bars represent SE. Letters on the bars indicate statistically different means ($P < 0.05$, ANOVA mixed model analysis, Tukey correction for multiple testing). See also Supplemental Data Set 4.

(G) to **(L)** Representative confocal images of *WOX5$_{pro}$:GFP-GUS* expressed in the wild type (**[G]** and **[J]**), *ccs52a2-1* (**[H]** and **[K]**), and *pkn2 ccs52a2-1* (**[I]** and **[L]**) primary roots at 5 (**[G]** to **[I]**) and 9 (**[J]** to **[L]**) DAS. The GFP signal is shown in green, while cell walls are visualized through PI staining (magenta). Arrows indicate the position of the quiescent center (QC), while ectopic *WOX5* expression in *ccs52a2-1* is indicated by arrowheads. Scale bars represent 25 μm. The number of roots imaged for each line and time point are shown in each image.

(**M**) and **(N)** Root length at 9 DAS of the wild type (WT), *cyca3;1*, *ccs52a2-1*, and *cyca3;1 ccs52a2-1* ($n \geq 12$) **(M)** or of WT, *cyca3;2*, *ccs52a2-1*, and *cyca3;2 ccs52a2-1* ($n \geq 9$) **(N)**. Plants were genotyped and measured in segregating F2 populations. Bars represent the mean, and error bars represent SE. Letters on the bars indicate statistically different means ($P < 0.05$, ANOVA, Tukey correction for multiple testing). See also Supplemental Data Set 4.

putative targets or regulators of the APC/C^{CCS52A2} ubiquitin ligase complex through a mutagenesis revertant screen. Therefore, EMS-mutagenized *ccs52a2-1* plants were screened in the M_2 generation for a recovered root growth. Out of a total of 260 initially identified revertants, 33 were confirmed in the next generation. Among these, one revertant mutation, named *pikmin2* (*pkn2*), yielded a root length in between that of wild-type and *ccs52a2-1* mutant plants (Figures 1A to 1C; Supplemental Figures 1A to 1C).

Root growth of the *ccs52a2-1* mutant was found to be strongly reduced during early development, showing a primary root growth rate of only around 20% of that of wild-type plants from 3 to 5 d after stratification (DAS; Figure 1E). At later time points, the root growth rate of the *ccs52a2-1* mutant gradually recovered but never fully caught up to that of wild-type plants. At 9 DAS, the *ccs52a2-1* root length was ~40% of that of wild-type plants (Figure 1F). Compared to the *ccs52a2-1* mutant, the *pkn2 ccs52a2-1* double mutant showed an increased root growth rate over the total time frame measured (Figure 1E), resulting in a root length recovery to 67% of that of wild-type plants at 9 DAS (Figure 1F). The root growth phenotype of *ccs52a2-1* was reflected in the root meristem length measured at 9 DAS, reaching only 78% of the wild type, primarily caused by a reduction in cell number, as cell size was not significantly altered (Figure 1F). In the *pkn2 ccs52a2-1* double mutant, root meristem length and cell number were slightly smaller but not significantly different from wild-type plants, nor was the cortical cell size (Figure 1F).

A striking characteristic of the *ccs52a2-1* mutant is a disorganized root stem cell niche, due to a loss of QC cell quiescence (Vanstraelen et al., 2009). To examine this phenotype in detail, a *WOX5$_{pro}$:GFP-β-glucuronidase* (*GUS*) transcriptional reporter

that marks the QC cells was introgressed into the *ccs52a2-1* and *pkn2 ccs52a2-1* mutant backgrounds. During early development (at 5 DAS), *WOX5* expression was detected in an expanded area of the disorganized QC and stem cell niche of the *ccs52a2-1* mutant, as well as in differentiated tissues such as the columella cells (Figures 1G and 1H; Supplemental Figures 1D and 1E). At a later developmental stage (9 DAS), *WOX5* expression was confined to the stem cell niche, coinciding with the partially recovered root growth phenotype, but still revealed a disorganized cell patterning (Figures 1J and 1K). Compared to the *ccs52a2-1* mutant, the *pkn2 ccs52a2-1* double mutant showed a slightly improved meristem organization at 5 DAS, together with a more confined *WOX5* expression domain (Figures 1H and 1I; Supplemental Figures 1E and 1F). At 9 DAS, its *WOX5* expression pattern more closely resembled that of wild-type plants (Figures 1J to 1L).

For the shoot tissue, a partial recovery of the *ccs52a2-1* phenotypes was seen in the *pkn2 ccs52a2-1* double mutant for the majority of parameters analyzed (Figure 1F). Projected rosette size of *ccs52a2-1* at 21 DAS was only 43% of that of wild-type plants, whereas that of the double mutant reached 83% (Figure 1F). This was reflected by the size of the first leaf pair at 21 DAS, with *ccs52a2-1* and *pkn2 ccs52a2-1* reaching 36% and 68% of wild-type leaf size, respectively (Figure 1F). Leaf growth recovery appeared to be mostly driven at the cell number level, with *ccs52a2-1* showing a reduction to 52% of wild-type epidermal cell number, whereas the *pkn2 ccs52a2-1* double mutant reached 89% (Figure 1F). No statistically significant recovery was seen in the epidermal cell size, with *ccs52a2-1* and *pkn2 ccs52a2-1* showing a similar reduction to 75% and 84% of that of wild type, respectively (Figure 1F). Furthermore, neither *ccs52a2-1* nor the double mutant showed a significant change in pavement versus stomatal cell ratio, as represented by the stomatal index (Figure 1F). As previously reported by Baloban et al. (2013), the number of endocycles, as represented by the endoreplication index, was reduced in the *ccs52a2-1* mutant to 75% of that of wild-type plants. A moderate recovery could be observed for the *pkn2 ccs52a2-1* double mutant, with an endoreplication index of 87% of that of wild-type plants (Figure 1F).

Identification of *cyca3;4* as *pkn2*

To identify the affected gene underlying the *pkn2* mutation, a mapping scheme was set up, in which the *pkn2 ccs52a2-1* mutant was backcrossed to the original *ccs52a2-1* parental line and subsequently self-pollinated. In the resulting segregating F2 mapping population, plants with the revertant long root phenotype were selected and pooled for gene mapping through next-generation sequencing, using the EMS-generated single-nucleotide polymorphisms (SNPs) as de novo mapping markers (see Methods for details). Plotting the distribution of the SNPs on the genome revealed a broad peak of increased mutant allele frequency in the middle of chromosome 1, and subsequently an interval of four million base pairs (Mbp) was selected for detailed analysis (from 13 Mbp to 18 Mbp; Supplemental Figure 2; Supplemental Table 1). After filtering for EMS-specific mutations with a concordance above 0.8 and filtering out intergenic or intronic mutations, only one candidate gene remained, namely *AT1G47230*, encoding the A-type cyclin CYCA3;4. The identified mutation was found to be located on the acceptor splice site of intron 5, changing the acceptor G base into an A (Figure 2A). Correspondingly, isolation of *CYCA3;4* transcript amplicons through RT-PCR identified two novel and distinct *CYCA3;4* splice variants within *pkn2 ccs52a2-1* (Figure 2B). Sequencing of these transcripts revealed that the longer variant retained the intron preceding the splice acceptor site mutation, while the shorter variant had both intron 5 plus 13 bp from the following exon spliced out (Figure 2A; Supplemental Figure 3). Cyclins generally contain two conserved cyclin folds, with the N-terminal fold responsible for binding to a CDK protein and the C-terminal fold responsible for target binding. Both expressed mRNA variants of *pkn2* resulted in a frame shift, leading to a premature stop codon and the loss of the second half of the predicted C-terminal cyclin fold of CYCA3;4 (Figure 2A), strongly suggesting that the mutant CYCA3;4 variants can no longer bind target proteins or perform their function.

Transformation of a complementation construct containing a functional copy of the *CYCA3;4* gene, *pFAST-R01-CYCA3;4*, into the *pkn2 ccs52a2-1* mutant confirmed that the *pkn2* mutation in *CYCA3;4* was responsible for the recovery of the *ccs52a2-1* root growth phenotype, as out of the 135 transformants obtained, 123 reverted to the stunted root growth phenotype (Figure 1D). Remarkably, many transformants grew even worse than *ccs52a2-1* plants, suggesting that the root growth phenotype of the *ccs52a2-1* plants might be strongly linked with CYCA3;4 abundance and that timely breakdown of CYCA3;4 might be essential for proper plant development.

As independent proof that *CYCA3;4* deficiency rescues the *ccs52a2-1* phenotype, independent *CYCA3;4* mutants obtained from insertion collections were selected. Two lines, SALK_204206 and SALK_061456, named *cyca3;4-2* and *cyca3;4-3* in accordance with regarding *pkn2* as *cyca3;4-1*, were found to hold a T-DNA insertion within the first intron of the *CYCA3;4* gene that resulted in a very strong reduction of transcript abundance (Figure 2A; Supplemental Figures 4A and 4B). Both T-DNA insertion mutants were analyzed for different root and shoot parameters but did not show any significant phenotypic differences from wild-type plants (Supplemental Figure 4C). However, when the *cyca3;4-2* mutant was introgressed into the *ccs52a2-1* background, the resulting *cyca3;4-2 ccs52a2-1* double mutant largely phenocopied the *pkn2 ccs52a2-1* double mutant in respect to the measured root and leaf growth parameters (Figures 1E and 1F), displaying a partial recovery of the *ccs52a2-1* root length and meristem size, leaf size, leaf epidermal cell number, and endoreduplication phenotypes, albeit slightly less pronounced when compared to *pkn2 ccs52a2-1*.

CYCA3;4 is part of a four-member family of closely related genes (*CYCA3;1* to *CYCA3;4*). Whereas *CYCA3;3* appears to be meiosis specific, *CYCA3;1*, *CYCA3;2*, and *CYCA3;4* are expressed in the root tip (Bulankova et al., 2013). Therefore, we tested whether absence of *CYCA3;1* or *CYCA3;2* also enabled the rescue of the *ccs52a2-1* mutant phenotype. For this, available homozygous *CYCA3;1* and *CYCA3;2* T-DNA insertion lines (Takahashi et al., 2010) were crossed with the homozygous *ccs52a2-1* mutant. Plants from the segregating F2 populations were genotyped and their root lengths measured. Similar to the two *CYCA3;4* insertion mutants, no root growth phenotype was observed for the *CYCA3;1* or *CYCA3;2* single mutants (Figures 1M

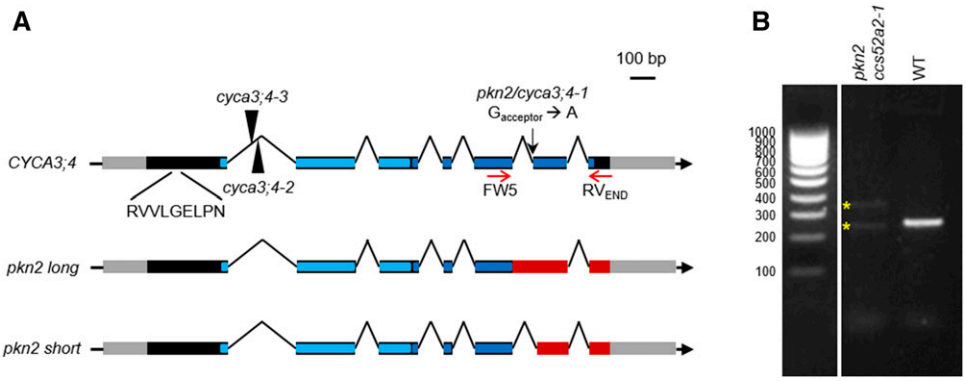

Figure 2. The *CYCA3;4* Gene Structure.

(A) The gene structure of the wild-type *CYCA3;4* gene, showing the location of the EMS mutation (black arrow), T-DNA insertions (arrowheads), and D-box sequence. The two splice variants created through the *pkn2* mutation are shown below. The gray and black boxes represent the untranslated regions and the coding sequences, respectively, while the lines represent the intergenic sequences and introns. The predicted N- and C-terminal cyclin folds are indicated in light and dark blue, respectively. In the mutant variants, the out-of-frame sequences are indicated in red.

(B) RT-PCR on whole-seedling cDNA of *pkn2 ccs52a2-1* and wild type (WT; Col-0) using *CYCA3;4* primers FW5 and RV_{END} (represented by red arrows in **[A]**), and, whereas only one amplicon was detected for the WT, two distinct amplicons were detected for the revertant (yellow stars), representing two newly created splice variants.

and 1N). Moreover, contrary to what was observed for *CYCA3;4*, a lack of *CYCA3;1* or *CYCA3;2* did not result in a rescue of the *ccs52a2-1* short root phenotype (Figures 1M and 1N).

CCS52A2 Targets CYCA3;4 for Degradation

CYCA3;4 is likely a direct target for APC/C^{CCS52A2}-dependent ubiquitination and subsequent proteasomal degradation, as it holds the full D-box sequence RVVLGELPN (Figure 2A), which serves as a binding site recognition motif for the APC/C (da Fonseca et al., 2011). To test this hypothesis, a previously described *CYCA3;4$_{pro}$:CYCA3;4-GUS* translational reporter line (Bulankova et al., 2013) was treated with the proteasome inhibitor MG-132. For comparison, the corresponding translational reporter of *CYCA3;1* (*CYCA3;1$_{pro}$:CYCA3;1-GUS*) and of *CYCA3;2* (*CYCA3;2$_{pro}$:CYCA3;2-GUS*) were included. Following a short GUS staining, CYCA3;1-GUS activity was barely visible in the root tip, whereas CYCA3;2-GUS and CYCA3;4-GUS could be detected in the root transition zone (Figures 3A, 3C, and 3E). After a 24-h treatment with MG-132, an increase in GUS activity could be observed in the root transition zone for CYCA3;1-GUS (Figure 3B). This increase was more pronounced for CYCA3;2-GUS and CYCA3;4-GUS, showing stronger staining in not only the transition zone but also the root meristem (Figures 3D and 3F). The accumulation of CYCA3;2-GUS and CYCA3;4-GUS in the root meristem corresponded to the spatial expression pattern of *CCS52A2*, whereas expression of *CCS52A1* was confined to the root transition zone (Supplemental Figure 5; Vanstraelen et al., 2009; Liu et al., 2012). These data suggest that CYCA3;1 might mostly be targeted for degradation by APC/C^{CCS52A1}, whereas CYCA3;2 and CYCA3;4 might be controlled by both APC/C^{CCS52A1} and APC/C^{CCS52A2}. To rule out that the effect seen is due to a change in *CYCA3;4* transcription, MG-132 was applied to root tips of a *35S$_{pro}$:CYCA3;4-GFP* reporter line, yielding increased levels of GFP fluorescence in the root meristem, independently demonstrating that CYCA3;4 protein levels are subject to proteasome-dependent regulation (Supplemental Figure 6).

To confirm the hypothesis that CYCA3;4 is marked for breakdown by CCS52A2 in the root meristem, the *CYCA3;1$_{pro}$:CYCA3;1-GUS*, *CYCA3;2$_{pro}$:CYCA3;2-GUS*, and *CYCA3;4$_{pro}$:CYCA3;4-GUS* reporters were introgressed into the *ccs52a2-1* mutant background. While the growth of plants harboring a mutation in *CCS52A2* and homozygous for *CYCA3;1$_{pro}$:CYCA3;1-GUS* was not significantly different from that of *ccs52a2-1* mutant plants, growth was reduced by around 40% for *CYCA3;2$_{pro}$:CYCA3;2-GUS* and, most strikingly, almost completely stalled for *CYCA3;4$_{pro}$:CYCA3;4-GUS* (Figures 4A to 4E and 4L). This is most probably due to the extra CYCA3;2 or CYCA3;4 protein present because of the reporter construct, again highlighting the importance for plant development of the timely breakdown of CYCA3;2 and especially CYCA3;4 by *ccs52a2-1*. Comparing the GUS activity of the three reporter constructs in wild-type versus *ccs52a2-1* mutant plants revealed that the spatial accumulation pattern of CYCA3;1-GUS was largely maintained in the shortened *ccs52a2-1* meristem (Figures 4F and 4G). Contrastingly, both CYCA3;2-GUS and CYCA3;4-GUS staining appeared to be stronger at the most distal part of the root meristem (Figures 4H to 4K). Taken together, this indicates that of the three A3-type cyclins, CYCA3;4 is the most important target of APC/C^{CCS52A2} in root development.

Previously, *CYCA3;1* and *CYCA3;2* transcript levels were demonstrated to be upregulated during the S phase, while *CYCA3;4* was found to be constitutively expressed during the cell cycle (Takahashi et al., 2010). To identify the cell cycle phase during which the cyclin proteins might be targeted for destruction, root tips of the *CYCA3-GUS* translational reporter lines were synchronized using hydroxyurea and histochemically stained after 6, 10, 17, and 20 h, representing time points with a majority of the meristematic cells residing in the S, G_2, G_2/M, or M/G_1 phase, respectively (Cools et al., 2010). Compared to control conditions

at 0 h, an increased GUS staining could be seen after 6 and 10 h of hydroxyurea treatment for CYCA3;1-GUS and CYCA3;2-GUS, followed by a drop in intensity at 17 and 20 h (Figures 5A to 5J). Contrastingly, CYCA3;4-GUS staining was most intense at the 17-h time point and appeared mostly similar to control conditions for all the other time points (Figures 5K to 5O). These data indicate that the distinct CYCA3 proteins accumulate differently throughout the cell cycle, with CYCA3;1 and CYCA3;2 being predominantly present during the S and G_2 phases, whereas CYCA3;4 appears to accumulate during the late G_2 or early M phase.

To more precisely pinpoint the cell cycle phase during which CYCA3;4 would be targeted for destruction by APC/$C^{CCS52A2}$, the CYCA3;4-GUS protein abundance in the root tip was analyzed through an immunostaining experiment using an anti-GUS antibody. In wild-type plants, a positive CYCA3;4-GUS signal could only be detected in nuclei of prophase cells (Figure 6A; Supplemental Table 2). By contrast, in the *ccs52a2-1* mutant background, CYCA3;4-GUS could additionally be detected in metaphase and anaphase nuclei (Figure 6B; Supplemental Table 2), demonstrating that CYCA3;4 is targeted for destruction by APC/$C^{CCS52A2}$ in postprophase cells.

Moderate *CYCA3;4* Overexpression Induces Unscheduled Formative Divisions in the Root Meristem, Whereas High Overexpression Inhibits Cell Division

The data suggested that CYCA3;4 abundance needs to be strictly controlled, as its stabilization in postprophase cells appears to trigger a growth arrest. Therefore, to study the effects of increased CYCA3;4 levels in more detail, we generated overexpression lines expressing the *CYCA3;4* gene from the strong *Cauliflower mosaic virus* (*CaMV*) *35S* promoter (*CYCA3;4*^{OE}). Overexpression levels in the root tip ranged between two- and eightfold compared to wild-type levels (Supplemental Figure 7A), whereas in the young shoot relative overexpression levels were higher, varying between 16- and 29-fold (Supplemental Figure 7B). Homozygous plants were generally smaller but appeared to be prone to tissue- and development-dependent silencing of the overexpression construct, as evidenced by the difference in penetrance of the observed phenotypes (Supplemental Figure 7C). This silencing could be reverted by crossing with wild-type plants, generating hemizygous lines. Therefore, to be able to see the effect of both moderate and high levels of overexpression, analysis in the root was performed on homozygous lines 11.2 and 12.4, which showed partial silencing of the overexpression construct, as well as on hemizygous plants resulting from crossing the respective lines with wild-type plants. Initially, following germination, root growth in both the homozygous and hemizygous *CYCA3;4*^{OE} lines was similar to that of wild-type plants but subsequently became slower, most prominently observed in the hemizygous lines, resulting in a significant reduction in total root length at 9 DAS (Figures 7A and 7B). This reduced growth was accompanied by a decrease in root meristem length, which was more drastic for the hemizygous lines (Figures 7C and 7D). This shortening was found to be fully due to a decrease in meristem cell number, as cell size remained unchanged (Figures 7C and 7D). Interestingly, an aberrant division pattern reminiscent to that of *ccs52a2-1* mutant roots could be detected in the majority of the measured roots of the

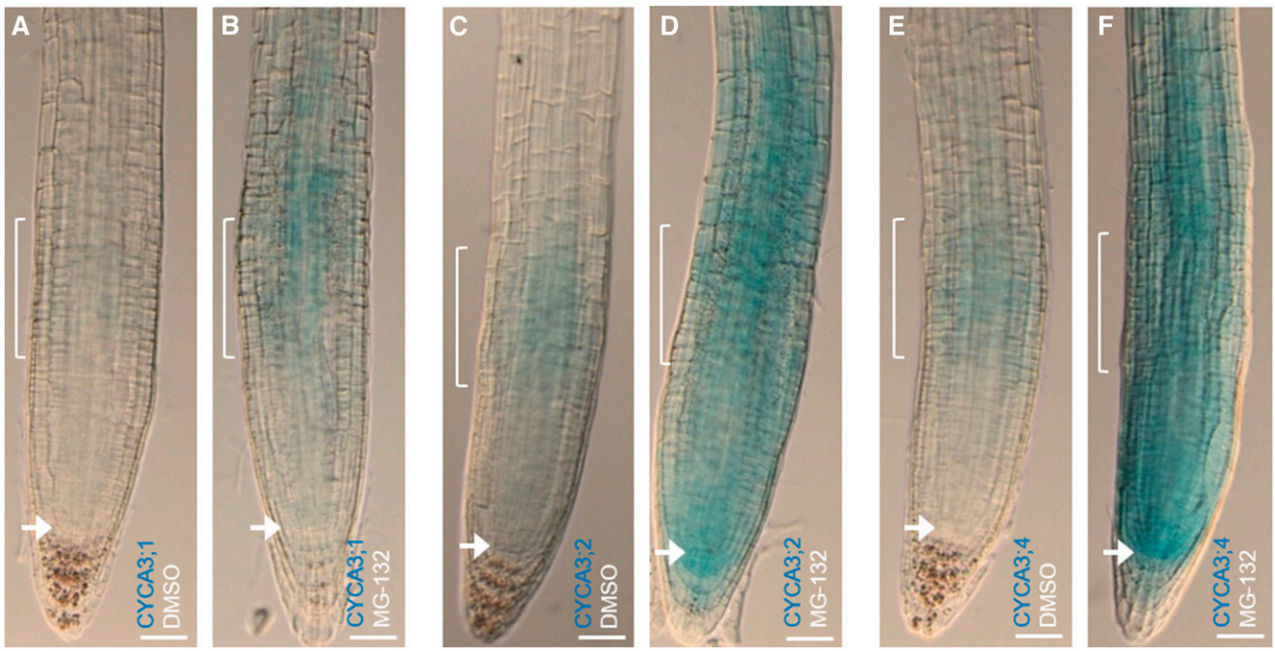

Figure 3. CYCA3;1, CYCA3;2, and CYCA3;4 Protein Levels Are Dependent on Proteasomal Degradation.

(A) to **(F)** Histochemical GUS staining of *CYCA3;1*$_{pro}$*:CYCA3;1-GUS* (**[A]** and **[B]**), *CYCA3;2*$_{pro}$*:CYCA3;2-GUS* (**[C]** and **[D]**), and *CYCA3;4*$_{pro}$*:CYCA3;4-GUS* (**[E]** and **[F]**) root tips at 5 DAS after a 24-h treatment with DMSO control (**[A]**, **[C]**, and **[E]**) or with the proteasome blocker MG-132 (**[B]**, **[D]**, and **[F]**). The transition zone and the QC are indicated by brackets and arrows, respectively. Roots were stained for 30 min. Scale bars represent 50 μm.

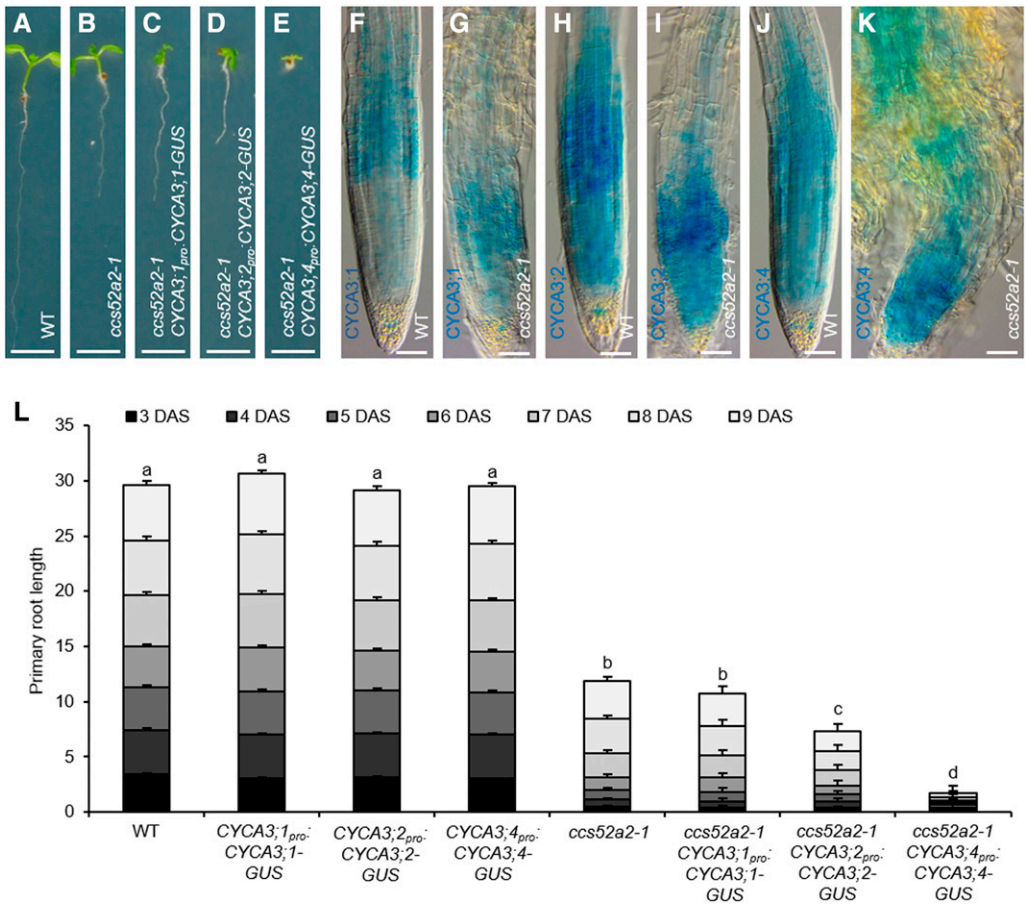

Figure 4. The *CYCA3$_{pro}$:CYCA3-GUS* Constructs in the *ccs52a2-1* Background.

(A) to **(E)** Representative seedlings of the wild type (WT) **(A)**, *ccs52a2-1* **(B)**, and *ccs52a2-1* with *CYCA3;1$_{pro}$:CYCA3;1-GUS* **(C)**, *CYCA3;2$_{pro}$:CYCA3;2-GUS* **(D)**, or *CYCA3;4$_{pro}$:CYCA3;4-GUS* **(E)** at 9 DAS. Scale bars represent 5 mm.

(F) to **(K)** Histochemical GUS staining at 5 DAS of wild type (WT; **[F]**, **[H]**, and **[J]**) and *ccs52a2-1* knockout (**[G]**, **[I]**, and **[K]**) root tips with either *CYCA3;1$_{pro}$:CYCA3;1-GUS* (**[F]** and **[G]**), *CYCA3;2$_{pro}$:CYCA3;2-GUS* (**[H]** and **[I]**), or *CYCA3;4$_{pro}$:CYCA3;4-GUS* (**[J]** and **[K]**) constructs in their background. Roots were stained for 2 h. Pictures were taken at the same magnification. Scale bars represent 50 μm.

(L) Primary root length of the respective *CYCA3$_{pro}$:CYCA3-GUS* lines in the wild-type (WT) and *ccs52a2-1* background from 3 to 9 DAS. Bars represent estimated marginal means, and bar heights were subdivided according to the measured daily growth. Error bars represent SE ($n \geq 23$), and letters indicate statistically different means for each genotype, as calculated for the total root length at 9 DAS ($P < 0.05$, ANOVA mixed model analysis, Tukey correction for multiple testing). See also Supplemental Data Set 4.

homozygous lines, whereas the cell pattern in the highly overexpressing hemizygous lines appeared normal (Figures 7E to 7J). Taken together, these data indicate that moderate overexpression of *CYCA3;4* induces unscheduled formative divisions, whereas high overexpression inhibits cell division altogether.

CYCA3;4 Overexpression Severely Affects Leaf Cell Differentiation

Although homozygous *CYCA3;4^{OE}* lines 11.2 and 12.4 showed a strongly reduced rosette size, the size of the first leaf pair was only slightly reduced, indicating age-dependent silencing of the overexpression construct (Supplemental Figure 7B). Therefore, we focused on the strongly overexpressing *CYCA3;4^{OE}* hemizygous lines 11.2 and 12.4 for leaf phenotyping, in which maintenance of *CYCA3;4* overexpression was confirmed through RT-qPCR (Supplemental Figure 8A). The size of both the whole rosette as well as the first leaf pair was dramatically reduced within both independent lines to less than 20% of that of wild-type plants (Figure 8A). This reduction was due to a lack of cell growth, as pavement cells were round and small (Figures 8B to 8D), with their size reduced to only ~5% of that of wild-type cells (Figure 8A). Concurrently, endoreplication was also strongly suppressed in both hemizygous lines (Figure 8A). Interestingly, while pavement cell number was increased (Figure 8A), an almost complete lack of stomata could be observed. Likewise, a less severe but significant reduction in stomatal density was observed in all homozygous lines (Supplemental Figure 7C). The observed reduction in stomatal number was accompanied by an increase in the transcripts of *SPCH*, a gene controlling the early steps of stomata formation

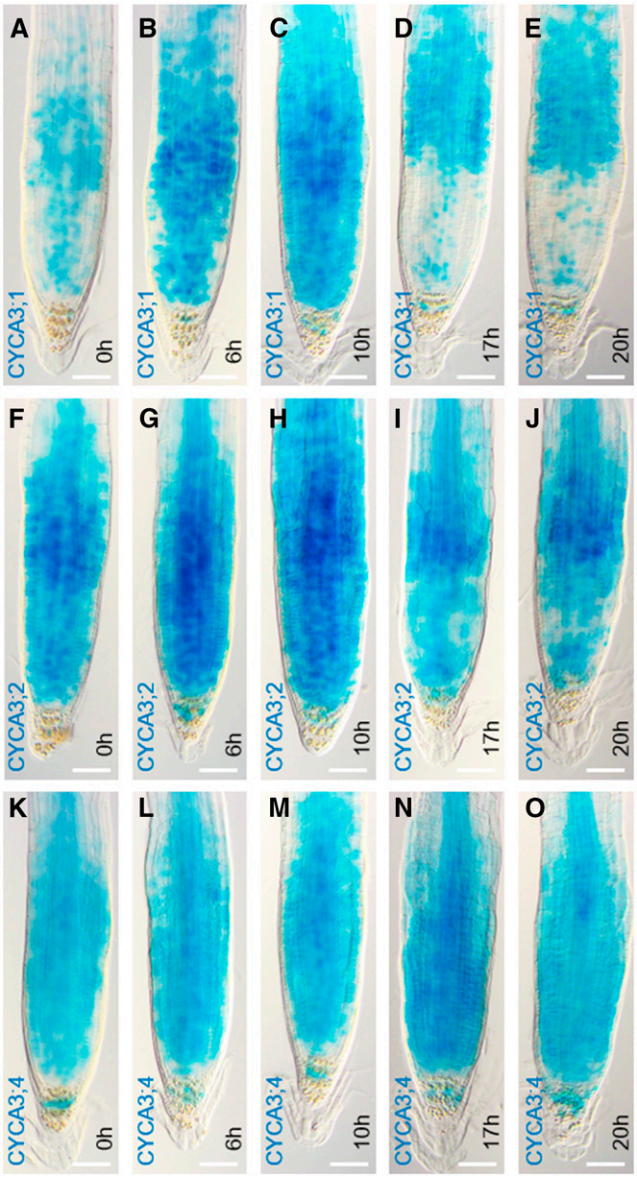

Figure 5. Accumulation of CYCA3 Proteins throughout the Cell Cycle.

(A) to **(O)** GUS signal at 7 DAS in root tips of *CYCA3;1*$_{pro}$*:CYCA3;1-GUS* (**[A]** to **[E]**), *CYCA3;2*$_{pro}$*:CYCA3;2-GUS* (**[F]** to **[J]**), and *CYCA3;4*$_{pro}$*:CYCA3;4-GUS* (**[K]** to **[O]**) synchronized by treating with 2 mM hydroxyurea for the indicated periods. The 0-h time point represents untreated control conditions (**[A]**, **[F]**, and **[K]**), while 6 h corresponds with S phase (**[B]**, **[G]**, and **[L]**), 10 h with G_2 (**[C]**, **[H]**, and **[M]**), 17 h with G_2/M (**[D]**, **[I]**, and **[N]**), and 20 h with M/G_1 (**[E]**, **[J]**, and **[O]**). Per line and time point, six images were taken. Scale bars represent 50 μm.

(Figure 8H), while the expression of the late stomatal development pathway gene *FAMA* was not significantly altered (Figure 8I). A role for CYCA3;4 in the early steps of stomatal development could be confirmed by GUS staining of young seedlings of a *CYCA3;4*$_{pro}$*:EGFP-GUS* line, revealing a specific GUS signal in the stomatal precursor cells (Figure 8J).

Ectopic *CCS52A2* Expression Partially Counteracts the Leaf *CYCA3;4* Overexpression Phenotypes

Following the hypothesis that CYCA3;4 is targeted for proteasomal degradation by APC/$C^{CCS52A2}$, it could be reasoned that the *CYCA3;4*^{OE} phenotypes could be counteracted by co-overexpression of *CCS52A2*. To test this, *CYCA3;4*^{OE} lines 11.2 and 12.4 were crossed with a mild *CCS52A2*^{OE} line (Baloban et al., 2013), and growth characteristics were subsequently analyzed in the first-generation progeny. To rule out the effect of silencing on *CYCA3;4* transcript overabundance, overexpression of *CYCA3;4* and *CCS52A2* was confirmed by RT-qPCR (Supplemental Figures 8A and 8B). The *CYCA3;4*^{OE} *CCS52A2*^{OE} co-overexpressing lines showed a significant recovery of growth compared to the single *CYCA3;4*^{OE} lines, as seen in rosette growth, first leaf pair size, and endoreplication index (Figure 8A). The increase in leaf size was due to an increase in pavement cell number compared to single *CYCA3;4*^{OE} plants and a simultaneous increase in pavement cell size, showing again a more puzzle piece-like shape (Figures 8A and 8E to 8G). Additionally, although still limited in number, stomatal guard cells could be observed, accompanied by a normalization of transcript levels of *SPCH* (Figure 8H). These results indicate that the growth recovery seen in double-overexpressing plants is due to an increased targeting of the overabundant CYCA3;4 protein for proteasomal degradation by the APC/$C^{CCS52A2}$.

CYCA3;4 Might Function through RBR1 Phosphorylation

To identify potential targets for CYCA3;4-dependent CDK phosphorylation, a phosphoproteomics assay that discovers differentially phosphorylated proteins was performed on three pools of 14-DAS-old seedlings of the hemizygous *CYCA3;4*^{OE} line 11.2. A total of 56 differentially phosphorylated peptides were identified among 54 different proteins, of which 17 phosphopeptides from 16 proteins showed enhanced phosphorylation in the *CYCA3;4*^{OE} background compared to the wild type, whereas 39 phosphopeptides from 38 proteins displayed reduced phosphorylation (Figure 9A; Supplemental Data Sets 1 and 2). Furthermore, 28 phosphopeptides from 24 proteins were identified in only one genotype and were designated "unique," with 19 phosphopeptides from 15 proteins only identified in wild-type plants and nine only identified in the *CYCA3;4*^{OE} background (Supplemental Data Set 3). Interestingly, 22 of the 26 phosphopeptides (i.e., 84.6%), being more abundantly phosphorylated in or unique for *CYCA3;4*^{OE}, contained the minimal CDK phosphorylation sites Ser-Pro or Thr-Pro ([S/T]P), and out of those, four were part of the full CDK phosphorylation site Ser/Thr-Pro-X-Lys-Arg ([S/T]Px[K/R]; Figure 9B).

Among the proteins showing increased phosphorylation, histone 1.2 (H1.2, AT2G30620) and RETINOBLASTOMA-RELATED1 (RBR1) could be found. For the latter, two CDK phosphorylation consensus sites were identified: Thr406 phosphorylation was uniquely found in the overexpression background, whereas Ser911 was 2.75 times more phosphorylated in the *CYCA3;4*^{OE} background compared to the wild type (Figures 9C and 9D). Both sites are highly conserved throughout the plant and animal

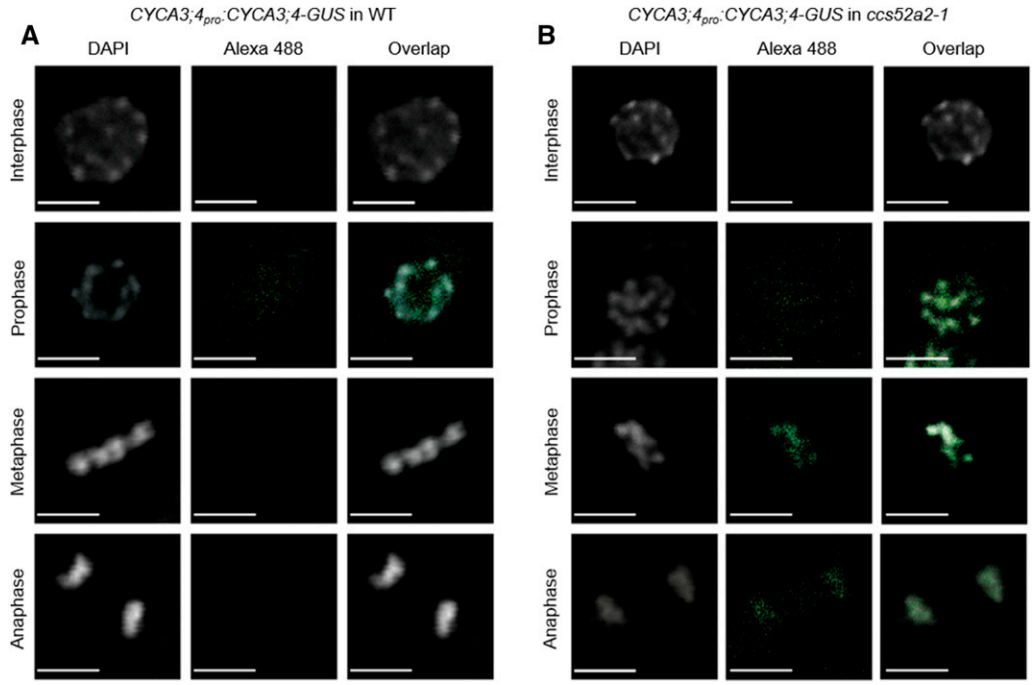

Figure 6. The Accumulation of CYCA3;4 Persists Past Prophase in the *ccs52a2-1* Background.

(A) and **(B)** Immunostaining of CYCA3;4-GUS throughout the cell cycle in squashed root tips of plants containing the *CYCA3;4$_{pro}$:CYCA3;4-GUS* construct in the wild-type **(A)** or *ccs52a2-1* **(B)** background. DNA was stained using 4′,6-diamidino-2-phenylindole (DAPI, gray) and CYCA3;4-GUS was visualized with a polyclonal rabbit anti-GUS primary antibody and an Alexa-488 secondary antibody (green). Scale bars represent 5 μm. See Supplemental Table 2 for quantification.

kingdoms, with Thr406 and Ser911 being part of a conserved TP and SPx[K/R] site, respectively (Figures 9E and 9F). To confirm the increase in RBR1 phosphorylation at Ser911, an immunoblot was performed on proteins extracted from root tips of the wild type and the *CYCA3;4^{OE}* homozygous line 12.4 using antibodies specifically targeting the phospho-Ser911 site and total RBR1. In both repeats, the ratio of S911-phosphorylated RBR1 to total RBR1 in the *CYCA3;4*-overexpressing background was twice that of the ratio in the wild type (Figures 9G and 9H).

DISCUSSION

CCS52 proteins play an important role in restraining cell division through the stimulation of proteolytic turnover of proteins during the cell cycle. CCS52A2 in particular has a key function in preventing unscheduled stem cell divisions, as its deficiency results in a distorted stem cell niche, both in the root and shoot (Vanstraelen et al., 2009; Liu et al., 2012). Despite its developmental importance, the number of known or potential APC/C^{CCS52A2} targets is limited. Here, we identified, through a suppressor screen, the CYCA3;4 protein as a likely proteolytic APC/C^{CCS52A2} target with an important role in controlling stem cell divisions. Knockout of *CYCA3;4* in the *ccs52a2-1* mutant background partially rescued the stem cell organization and root growth phenotypes, as well as leaf cell division defects. The data imply that the inability to control the CYCA3;4 protein level is one of the underlying reasons for the *ccs52a2-1* mutant phenotypes. Strikingly, introducing a *CYCA3;4* complementation construct in the *pkn2 ccs52a2-1* background or a translational reporter line within the *ccs52a2-1* mutant background predominantly resulted in an enhancement of the *ccs52a2-1* phenotype. We speculate that the origin of this enhanced phenotype might be the additional increase in CYCA3;4 abundance because of the introduction of one or more additional gene copies, again suggesting that that the level of CYCA3;4 abundance needs to be strictly controlled.

The evidence of CYCA3;4 being an APC/C^{CCS52A2} target is compelling. Not only does a mutation in *CYCA3;4* complement the *ccs52a2-1* phenotype, but co-overexpression with *CCS52A2* also suppresses the hyperproliferation phenotype of *CYCA3;4*-overexpressing plants. Moreover, CYCA3;4 was previously found to co-immunoprecipitate with CCS52A2 (Fülöp et al., 2005). Additionally, we found that the CYCA3;4$_{pro}$:CYCA3;4-GUS translational reporter protein predominantly accumulates in the distal root meristem following treatment with a proteasome inhibitor or when introduced within the *ccs52a2-1* mutant background, matching the spatial accumulation pattern of CCS52A2. Finally, through immunostaining, the CYCA3;4-GUS protein could be detected on the chromosomes of metaphase and anaphase cells within the *ccs52a2-1* mutant background, whereas in wild-type cells, the signal could only be detected in prophase nuclei. Next to strengthening the hypothesis that CYCA3;4 is an APC/C^{CCS52A2} target, these data also suggest that the APC/C^{CCS52A2} complex becomes active during mitosis, more precisely before metaphase.

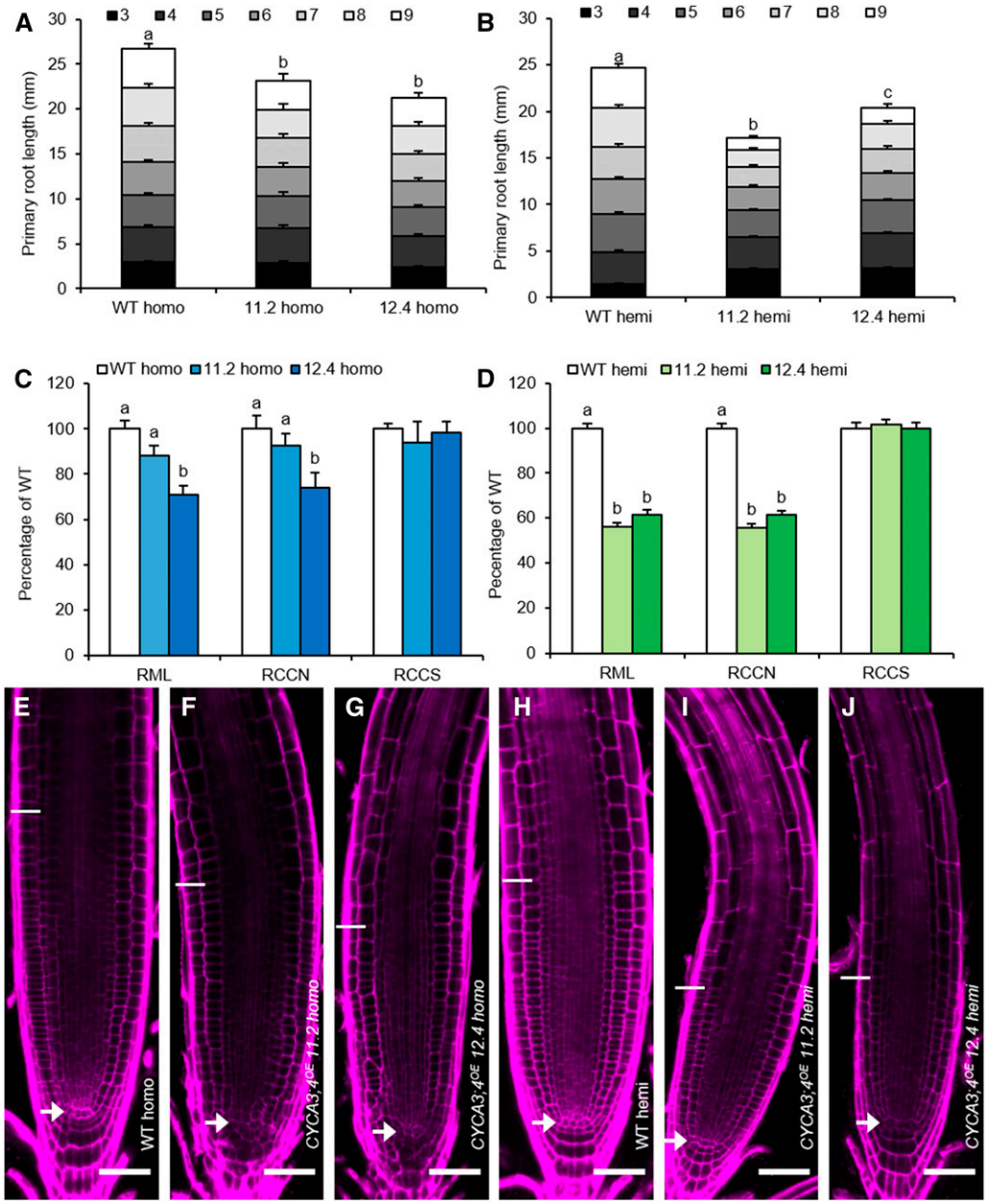

Figure 7. The Effects of *CYCA3;4* Overexpression in the Root.

(A) and **(B)** Primary root length from 3 to 9 DAS of homozygous (**[A]**, $n \geq 14$) and hemizygous (**[B]**, $n \geq 33$) *CYCA3;4*^{OE} lines 11.2 and 12.4. The bar heights were subdivided according to the measured daily growth. Bars represent estimated marginal means, error bars represent SE ($n \geq 23$), and letters indicate statistically different means for each genotype, as calculated for the total root length at 9 DAS ($P < 0.05$, ANOVA mixed model analysis, Tukey correction for multiple testing). See also Supplemental Data Set 4. WT, wild type.

(C) and **(D)** Root meristem characteristics at 9 DAS of homozygous (**[C]**, $n \geq 12$) and hemizygous (**[D]**, $n \geq 22$) *CYCA3;4*^{OE} lines 11.2 and 12.4. Bars represent estimated marginal means; error bars represent SE. Letters indicate statistically different means ($P < 0.05$, ANOVA mixed model analysis, Tukey correction for multiple testing). See also Supplemental Data Set 4. RML, Root meristem length; RCCN, root cortical cell number; RCCS, root cortical cell size; WT, wild type.

(E) to **(J)** Representative confocal images of the root meristem of homozygous (**[E]** to **[G]**) or hemizygous (**[H]** to **[J]**) wild type (WT; **[E]** to **[H]**) and *CYCA3;4*^{OE} lines 11.2 (**[F]** to **[I]**) and 12.4 (**[G]** to **[J]**). Cell walls were visualized by PI staining. Arrows indicate the position of the QC, while the end of the meristem is indicated by a line. Scale bars represent 50 μm.

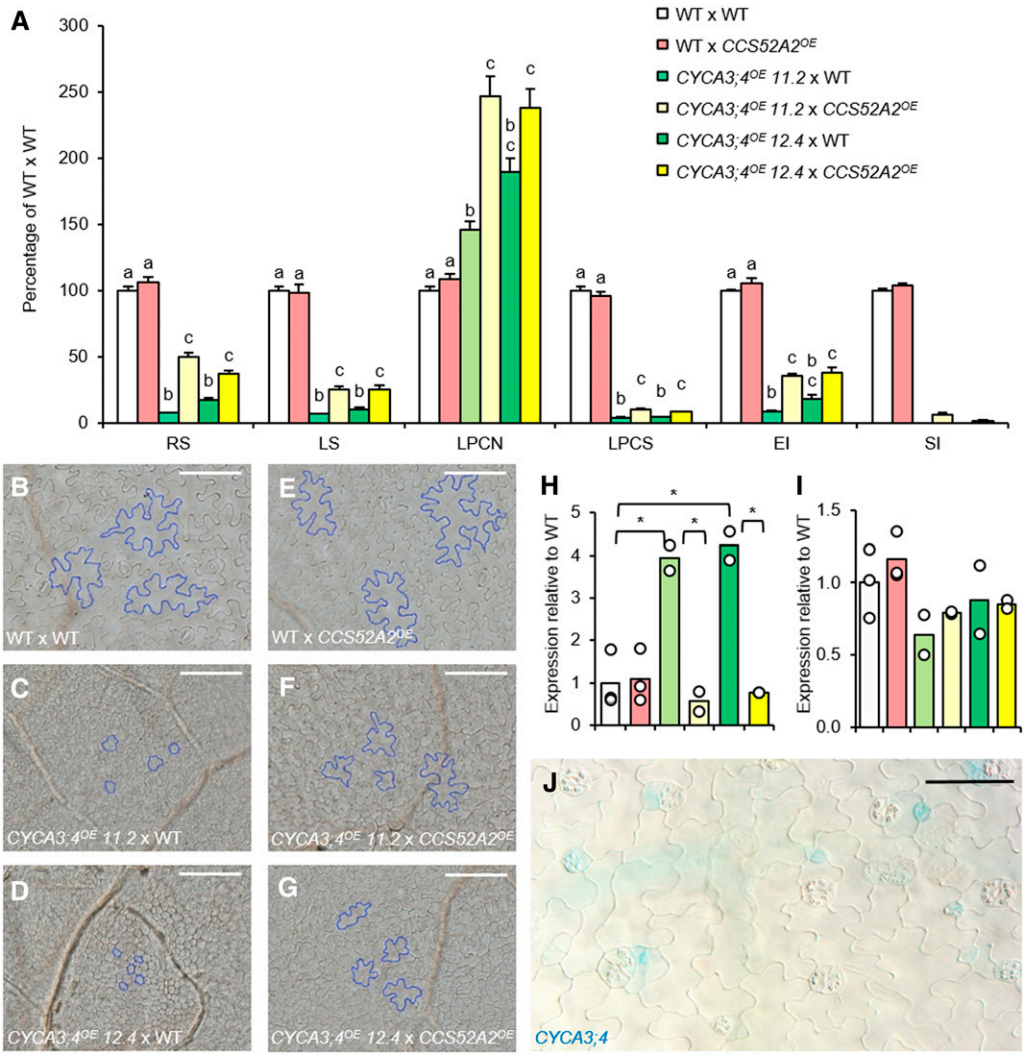

Figure 8. The Effects of Overexpression of *CYCA3;4* and Co-overexpression of *CCS52A2* in the Leaf.

(A) Shoot phenotyping at 21 DAS of hemizygous first-generation progeny resulting from crosses between wild type, *CYCA3;4*^{OE} line 11.2 or line 12.4 and wild type or *CCS52A2*^{OE}. RS, Rosette size ($n \geq 21$); LS, leaf size of the first leaf pair ($n \geq 11$); LPCN, leaf pavement cell number ($n \geq 5$); LPCS, leaf pavement cell size ($n \geq 5$); EI, endoreplication index ($n \geq 5$); SI, stomatal index ($n \geq 5$). Bars represent means, and error bars represent SE ($n \geq 5$). Letters on the bars indicate statistically different means ($P < 0.05$, two-sample *t* tests with Bonferroni correction for multiple testing). See also Supplemental Data Set 4.

(B) to **(G)** Photomicrographs of the leaf epidermis, with some cells highlighted in blue to emphasize the change in cell size and shape, of the following crosses: wild type (WT) × WT **(B)**, *CYCA3;4*^{OE} *11.2* × WT **(C)**, *CYCA3;4*^{OE} *12.4* × WT **(D)**, WT × *CCS52A2*^{OE} **(E)**, *CYCA3;4*^{OE} *11.2* × *CCS52A2*^{OE} **(F)**, *CYCA3;4*^{OE} *12.4* × *CCS52A2*^{OE} **(G)**. Scale bars represent 50 μm.

(H) and **(I)** Expression levels of the stomatal development pathway genes *SPCH* **(H)** and *FAMA* **(I)** as measured by RT-qPCR in the first leaf pair at 21 DAS. Dots represent the measured values for each line ($n = 2$ or 3), while the bars represent the mean. See **(A)** for legend. Stars represent statistically different means ($P < 0,05$, two-sample *t* tests with Bonferroni correction for multiple testing). See also Supplemental Data Set 4.

(J) GUS staining of a 7-DAS-old cotyledon of *CYCA3;4*$_{pro}$*:EGFP-GUS*, showing staining in the stomatal precursor cells. Scale bar represents 50 μm.

Whereas knockout of *CYCA3;4* partially rescues the *ccs52a2-1* mutant phenotype, no obvious phenotypes could be observed upon loss of CYCA3;4 activity in a wild-type background, suggesting redundancy with other cyclins. *CYCA3;4* is part of a gene family holding four members. *CYCA3;4* (AT1G47230) itself is part of a tandem duplication also containing *CYCA3;2* (AT1G47210) and *CYCA3;3* (AT1G47220), whereas *CYCA3;1* (AT5G43080) resides on a different chromosome. The different chromosomal localization of *CYCA3;1* and *CYCA3;4* suggests genetic diversification, which can be seen in the distinct spatial and temporal accumulation patterns of their respective proteins. Whereas CYCA3;1 predominantly accumulates in the proximal root meristem, CYCA3;4 can also be detected in the stem cell region. Its presence in the upper meristem marks CYCA3;1 as a putative target for APC/C^{CCS52A1} rather than APC/C^{CCS52A2}, as CCS52A1 predominantly accumulates in the root at the beginning of the

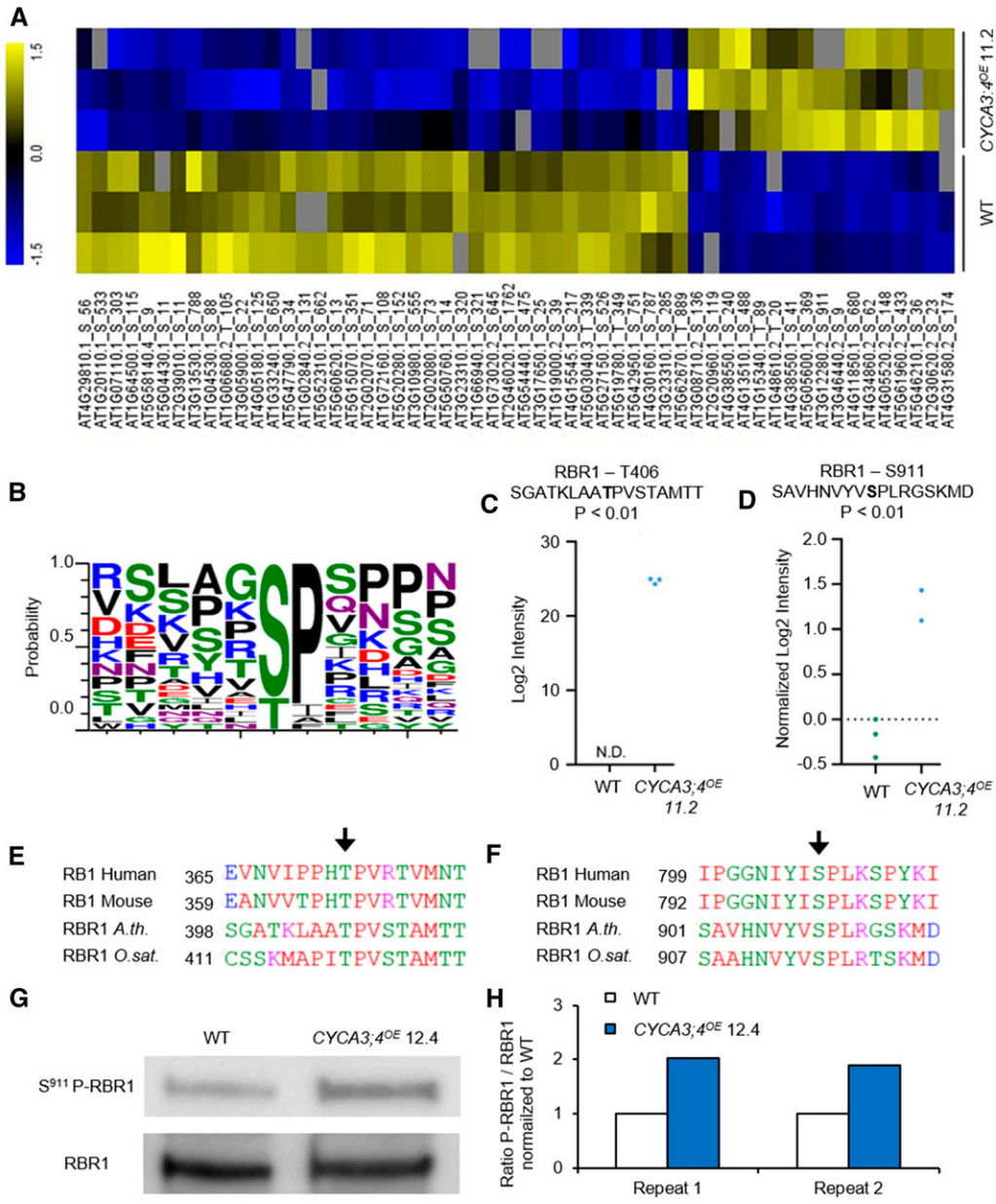

Figure 9. Phosphoproteomics Analysis in the *CYCA3;4*^{OE} Background.

(A) Hierarchical clustering of significantly regulated phosphopeptides from phosphoproteome profiling of *CYCA3;4*^{OE} versus Col-0 (Student's *t* test, P < 0.01). For each genotype, three biological replicates were sampled. Yellow and blue represent significantly up- and down-regulated phosphopeptides, respectively. Gray represents no signal detected. WT, wild type.

(B) Motif representing the occurrence of different amino acids in a ±5-amino-acid interval around the phosphorylated Ser or Thr in those sites showing increased phosphorylation in the *CYCA3;4*^{OE} background. Picture was made using the website http://weblogo.threeplusone.com/.

(C) and **(D)** Levels for the indicated RBR1 phosphopeptides in the wild-type (WT; green dots) and *CYCA3;4*^{OE} (blue dots) phosphoproteomes. Each dot represents a biological replicate. N.D., not detected.

(E) and **(F)** Conservation in plants and animals of phosphorylated sites Thr406 **(E)** and Ser911 **(F)** identified in Arabidopsis RBR1. Homologous proteins were identified using the STRING database (www.string-db.org) and aligned using the CLUSTAL OMEGA web tool (https://www.ebi.ac.uk/Tools/msa/clustalo/).

(G) Immunoblot of Ser911 phospho-RBR1 and RBR1, showing an increased amount of phosphorylated RBR1 in the *CYCA3;4*^{OE} background. WT, wild type.

(H) Quantification of the immunoblot shown in **(G)** and one additional repeat. Ratio of S911-phosphorylated RBR1 over unphosphorylated RBR1, normalized to the wild type (WT).

elongation zone, fitting with its role as a determinant of root meristem size (Vanstraelen et al., 2009). Correspondingly, a mutation in *cyca3;1* could not complement the *ccs52a2-1* phenotype, while the introduction of an extra *CYCA3;1* gene copy did not result in an enhanced *ccs52a2-1* root growth phenotype. These data suggest that CYCA3;1 is not a prominent APC/C^{CCS52A2} substrate. Functional diversification between CYCA3;1 and CYCA3;4 is also supported by their differential temporal protein accumulation pattern, with CYCA3;1 and CYCA3;4 peaking during the S and G_2/M phases, respectively.

CYCA3;3 appears to be meiosis specific, as no transcript or protein could be detected in nonmeiotic cells (Takahashi et al., 2010; Bulankova et al., 2013), leaving *CYCA3;2* as the most likely gene operating redundantly with *CYCA3;4*. However, although both CYCA3;2 and CYCA3;4 can be detected in the stem cell region and introducing a functional gene copy of *CYCA3;2* slightly enhanced the *ccs52a2-1* root growth phenotype, knockout of *CYCA3;2* did not complement the *ccs52a2-1* root length phenotype. Thus, although we cannot exclude a partial redundant role for *CYCA3;2* and *CYCA3;4* during the cell cycle, the complementation data suggest that only stabilization of CYCA3;4 contributes to the *ccs52a2-1* phenotype. Therefore, the inability to degrade proteins other than CYCA3;2 might account for the residual phenotypes of the *cyca3;4 ccs52a2-1* double mutants. Putative candidates include the ERF115 transcription factor and CSLD5, as both were shown to be under proteolytic control of APC/C^{CCS52A2} (Heyman et al., 2013; Gu et al., 2016). More recently, the OsSHR1 stem cell regulator was identified as a target of the rice CCS52A2 homolog (Lin et al., 2020), marking the Arabidopsis SHR protein as another potential target to be destroyed by APC/C^{CCS52A2} in order to maintain a functional root stem cell niche.

The need for controlled CYCA3;4 destruction is highlighted by the phenotypes triggered upon overexpression of the *CYCA3;4* gene, resulting in a small-leaf phenotype. Remarkably, no lines with very high *CYCA3;4* transcript levels could be obtained, and plants were prone to gene silencing, suggesting that strong overexpression might be counterselected for, a situation also seen upon overexpression of the *Nicotiana tabacum CYCA3;2* gene (Yu et al., 2003). The small-leaf phenotype of the *CYCA3;4*-overexpressing lines was mainly caused by a dramatic effect on cell size, being only partially offset by an increase in cell number. This makes the *CYCA3;4* overexpression phenotype different from that of the overexpression of other cyclins, such as *CYCD3;1*, in which the small-cell phenotype is accompanied by a 20- to 30-fold increase in epidermal cell number (Dewitte et al., 2003), whereas for *CYCA3;4*, only a maximum twofold increase in cell number was observed. Another major difference between *CYCD3;1*- and *CYCA3;4*-overexpressing lines is the lack of stomata in the latter, indicating that CYCA3;4 might affect the cell cycle in a unique way.

In addition to the small-leaf phenotype, *CYCA3;4*-overexpressing lines display an expression-level-dependent root meristem phenotype. Whereas more highly overexpressing lines only display a short root meristem phenotype due to a reduction in the number of meristem cells, the lines with a lower level of overexpression also display an increased frequency of aberrant divisions, including unscheduled periclinal divisions. Combined with the effect on stomata, this suggests that CYCA3;4 might play an important role in the process of formative cell divisions, which might correspond to the need for its destruction by APC/C^{CCS52A2} to obtain a well-organized stem cell niche. Its targeted destruction during early prophase, the moment when the division plane orientation is determined through positioning of the preprophase band (Rasmussen and Bellinger, 2018; Facette et al., 2019), fits the idea that CYCA3;4 and CCS52A2 might play a role in the positioning of the division plane. However, the phenotype of the *CYCA3;4*-overexpressing plants does not completely mimic that of the *ccs52a2-1* knockout, again suggesting that the stabilization of targets other than CYCA3;4 might account for a big part of the disorganized stem cell niche phenotype of *ccs52a2-1* plants.

Strikingly, two of the altered phenotypes observed, i.e. the stomata phenotype and the unscheduled stem cell divisions, are shared with plants silenced for the *RBR1* tumor suppressor gene (Wildwater et al., 2005; Borghi et al., 2010; Cruz-Ramírez et al., 2012; Matos et al., 2014). Reciprocally, hypomorphic *CDKA;1* mutants have been described to display delayed formative divisions in both the root and shoot, and this could be suppressed by a mutation in *RBR1* (Weimer et al., 2012). Because it is anticipated that phosphorylation by CDK proteins inhibits RBR1 activity (Harashima and Sugimoto, 2016), these data suggest that RBR1 inactivation induces formative divisions. Through our phosphoproteomics analysis of *CYCA3;4* overexpression plants, an enrichment for two phospho-sites within the RBR1 protein (T406 and S911) could be found. Both identified sites are part of the minimal CDK phosphorylation site [S/T]P and are highly conserved, corresponding to respectively T373 and S807 within the human RB protein, for which their phosphorylation has been demonstrated to reduce RB's inhibitory binding of E2F transcription factors (Ren and Rollins, 2004; Burke et al., 2010, 2012, 2014). Assuming that the phosphorylation of RBR1 triggers an identical effect, it might be speculated that CYCA3;4 in complex with CDKA;1 might regulate stem cell identity or polarity of cell divisions through inhibition of RBR1 and that this activity is restrained through APC/C^{CCS52A2} activity. Furthermore, as only a limited number of proteins were found to display increased phosphorylation upon *CYCA3;4* overexpression, RBR1 might be the main target of CYCA3;4. However, we currently do not have biochemical evidence that RBR1 is a direct target of a CYCA3;4-CDKA;1 pair, as through interaction experiments we failed to detect direct binding between RBR1 and CYCA3;4, fitting with the absence of an LxCxE RBR1 interaction motif in CYCA3;4. Therefore, it currently cannot be excluded that the increase in RBR1 phosphorylation might be an indirect consequence of the strong phenotypic effects of *CYCA3;4* overexpression. Interestingly, expression of the *CCS52A* genes is under direct negative control of RBR1 (Magyar et al., 2012), leading to the possibility that CYCA3;4 might be responsible for triggering its own APC/C^{CCS52A2}-mediated breakdown through the phosphorylation and inactivation of RBR1. Conversely, RBR1 might regulate *CYCA3;4* expression, as the RBR1 protein was found to bind the *CYCA3;4* promoter (Bouyer et al., 2018). Combined with the shared phenotypes of the diverse gain- and loss-of-function lines, these data indicate that a complex interplay among CCS52A2, RBR1, and CYCA3;4 might lay at the basis of the spatial and temporal control of formative stem cell divisions.

METHODS

Plant Medium and Growth Conditions

Arabidopsis (*Arabidopsis thaliana*) seeds were sterilized in 70% (v/v) ethanol for 10 to 15 min and subsequently washed with 100% ethanol, after which they were left to dry in sterile conditions. For all experiments, the seeds were stratified in the dark for 2 d at 4°C before being placed in the respective growth rooms. Plants were grown in vitro under long-day conditions (16-h light/8-h dark, Lumilux Cool White lm, 50 to 70 μmol m^{-2} s^{-1}) at 21°C on solidified half-strength Murashige and Skoog medium (2.151 g/L), 10 g/L Suc, and 0.5 g/L MES, adjusted to pH 5.7 with 1 M KOH and 8 or 10 g/L agar. For analysis of root or shoot phenotypes, plants were grown vertically or horizontally, respectively. The drug treatments described were performed using the following conditions: MG132, 100 μM for 24 h, and hydroxyurea, 2 mM for the indicated time periods.

Constructs and Lines

The mutant lines *ccs52a2-1*, *cyca3;1*, and *cyca3;2* have been previously described by Vanstraelen et al. (2009) and Takahashi et al. (2010), whereas *cyca3;4-2* (SALK_204206) and *cyca3;4-3* (SALK_061456) were obtained from the Salk Institute T-DNA Express (Alonso et al., 2003) database. The *pkn2 ccs52a2-1* double mutant was obtained through EMS mutagenesis of *ccs52a2-1* mutant seeds (see below). The *$WOX5_{pro}$:GFP-GUS* transcriptional reporter was previously described by Heyman et al. (2016). The *CYCA3;4* complementation construct *pFAST-R01-CYCA3;4* was created by cloning a fragment containing the *CYCA3;4* promoter (1500 bp) and gene sequence (including introns) from Col-0 into the pDONR221 vector (Invitrogen) via BP reaction (Gateway, Invitrogen) and recombining it into the pFAST-R01 vector (Shimada et al., 2010) via LR reaction (Gateway, Invitrogen). The *$CYCA3;4^{OE}$* construct was created by cloning the *CYCA3;4* open reading frame from Col-0 into pDONR221 via BP reaction and subsequently recombining it via LR reaction behind the strong *Cauliflower mosaic virus* (*CaMV*) *35S* promoter in the pB7WG2 vector (Karimi et al., 2002). The *$35S_{pro}$:CYCA3;4-GFP* construct was created by cloning the *CYCA3;4* open reading frame (Col-0) without stop codon into pDONR221 via BP reaction and subsequently recombining it via LR reaction behind the *CaMV 35S* promoter and in front of GFP in the pK7FWG2 vector (Karimi et al., 2002). The *$CCS52A2^{OE}$* line was kindly donated by Eva Kondorosi (Baloban et al., 2013). The *$CYCA3;1_{pro}$:CYCA3;1-GUS, $CYCA3;2_{pro}$:-CYCA3;2-GUS* and *$CYCA3;4_{pro}$:CYCA3;4-GUS* translational reporter lines were kindly donated by Karl Riha (Bulankova et al., 2013). The *$CYCA3;4_{pro}$:EGFP-GUS* reporter was made by cloning a 1564-bp promoter fragment immediately upstream of the *CYCA3;4* gene into pDONR221 via BP reaction and recombining it via LR reaction into the pKGWFS7 vector (Karimi et al., 2002). The *$CCS52A1_{pro}$:CCS52A1-GUS* and *$CCS52A2_{pro}$:-CCS52A2-GUS* translational reporter constructs were created by cloning a fragment consisting of 2289 bp (for *CCS52A1*) and 2126 bp (for *CSS52A2*) of the sequence upstream of the start codon followed by the complete gene including introns but without stop codon into the pDONR-P4-P1r entry vector (Invitrogen) via BP reaction and cloning it in front of the GUS reporter (with intron and stop codon) by recombining it via LR reaction with pEN-L1-SI*-L2 into the pK7m24GW-FAST vector (Karimi et al., 2007; Shimada et al., 2010). All primer sequences used for cloning and genotyping are listed in Supplemental Table 3.

All vector-based cloning was performed using the Gateway system (Invitrogen). All constructs were transferred into the *Agrobacterium tumefaciens* C58C1RifR strain harboring the pMP90 plasmid. The obtained *Agrobacterium* strains were used to generate stably transformed Arabidopsis lines with the floral-dip transformation method (Clough and Bent, 1998). All constructs were transformed into the Col-0 background, except for the *CYCA3;4* complementation construct, which was transformed into *pkn2 ccs52a2-1*. Successful transformants were selected using kanamycin or basta (glufosinate ammonium) or using fluorescence microscopy in the case of FAST constructs. Double mutants were made by crossing and confirmed through genotyping with PCR and/or sequencing.

Plant Growth Phenotyping

Root growth and length were determined by marking the position of the root tip each day from 3 to 9 DAS, scanning the plates at 9 DAS and measuring using the ImageJ software package (https://imagej.net). Root meristem analysis was performed with the ImageJ software package using images of the root tip obtained with confocal microscopy, the distance between the QC and the end of the division zone was measured to determine the root meristem length, and the number of cortical cells within the division zone was counted to determine the cortical cell number.

For rosette size, pictures were taken at 21 DAS using a digital camera fixed in position, after which the images were made binary (black and white) and the projected rosette size was measured using the wand tool in ImageJ. For analysis of leaf parameters, the first leaf pairs were harvested at 21 DAS and cleared overnight using 100% ethanol. Next, leaves were mounted on a slide with lactic acid. The total leaf area was determined from images taken with a digital camera mounted on a Stemi SV11 microscope (Zeiss) using ImageJ. A DM LB microscope (Leica) with a drawing tube attached was used to generate a pencil drawing of a group of at least 30 cells of the abaxial epidermis. On each leaf, the area chosen for drawing was located between 25 and 75% of the distance between the tip and the base of the leaf, halfway between the midrib and the leaf margin. After measuring the total area drawn (using the wand tool of ImageJ) and counting the number of pavement cells and stomata drawn, the average cell size, total number of cells per leaf, and the stomatal index (number of stomata divided by total number of epidermal cells) were calculated.

Flow Cytometry

For flow cytometry analysis, leaf material was chopped in 200 μL nuclei extraction buffer, after which 800 μL staining buffer was added (Cystain UV Precise P, Partec). The mix was filtered through a 30-μm green CellTrics filter (Sysmex–Partec) and analyzed by the Cyflow MB flow cytometer (Partec). The Cyflogic software (http://www.cyflogic.com/) was used for ploidy measurements. To calculate the endoreplication index, the following formula was used, with %nC representing the fraction of nuclei with *n* times the haploid genome content:

$$(0 \times \%2C + 1 \times \%4C + 2 \times \%8C + 3 \times \%16C + 4 \times \%32C) \times /\text{Total nuclei}$$

Confocal Microscopy

For visualization of root apical meristems, vertically grown plants were mounted in a 10-μM propidium iodide (PI) solution (Sigma Aldrich) to stain the cell walls and imaged using an LSM 5 Exciter (Zeiss) confocal microscope. For PI and GFP excitation, the 543 line of a HeNe laser and the 488 line of an Argon laser were used, respectively. Laser light passed through an HFT 405/488/543/633 primary dichroic beamsplitter before reaching the sample and emitted light from the sample first passed through an NFT 545 secondary dichroic beamsplitter, after which it passed through a 650-nm longpass filter for PI detection and through a 505- to 530-nm bandpass filter for detection of GFP. PI and GFP were detected simultaneously with the line scanning mode of the microscope.

GUS Staining

Plants were grown for the indicated period and fixed in an ice-cold 80% (v/v) acetone solution for 3 h. Samples were washed three times with phosphate buffer (14 mM NaH_2PO_4 and 36 mM Na_2HPO_4) before being incubated in staining buffer (0.5 mg/mL 5-bromo-4-chloro-3-indolyl-β-D-glucuronic acid, 0.165 mg/mL potassium ferricyanide, 0.211 mg/mL potassium ferrocyanide, 0585 mg/mL EDTA pH 8, and 0.1% (v/v) Triton-X100, dissolved in phosphate buffer) at 37°C between 30 min and 16 h until sufficient staining was observed.

EMS Mutagenesis

Roughly 14,000 *ccs52a2-1* seeds were subjected to EMS mutagenesis. The seeds were first hydrated with water for 8 h on a rotating wheel before being mutagenized with a 0.25% (v/v) solution of EMS for another 12 h. After treatment, seeds were washed twice with 15 mL 0.1 M sodium thiosulfate ($Na_2S_2O_3$) for 15 min to stop the reaction and subsequently twice with water for 30 min. After that, seeds were left to dry on Whatman paper. Fifty-six pools of ~250 M_1 seeds were mixed together with fine sand in Eppendorf tubes and sown in big pots with standard soil. After selfing, M_2 seeds were harvested separately for every pool. Seeds were sterilized and sown on vertical plates to score for the reversion of the *ccs52a2-1* root growth phenotype. Plants with longer roots were subsequently selected and transferred to soil for self-fertilization. The recovery phenotype was then reconfirmed in the next generation (M_3).

Mapping of the Revertant Mutation

Segregating F2 progeny resulting from a cross between *pkn2 ccs52a2-1* and the *ccs52a2-1* parental line used for EMS mutagenesis was used as a mapping population. Approximately 250 plants showing the long root phenotype of the revertant were selected at 5 DAS and pooled for DNA extraction using the DNeasy plant mini kit (Qiagen) according to the manufacturer's instructions. DNA was extracted additionally from 200 plants of the original *ccs52a2-1* parental line. Illumina True-Seq libraries were generated from the extracted DNA according to the manufacturer's protocol and sequenced on an Illumina HiSeq 100-bp paired-end run. The SHORE pipeline (Ossowski et al., 2008) was used for the alignment of sequences of both *pkn2 ccs52a2-1* and *ccs52a2-1* to the reference genome (Col-0; The Arabidopsis Information Resource 10). Using the SHOREmap pipeline (Sun and Schneeberger, 2015), an interval of increased mutant SNP alleles was identified and subsequently annotated. Filtering was performed within the interval for de novo EMS-specific (G to A or C to T) SNPs with a concordance above 0.8 and intergenic or intronic mutations were removed to reveal the potential revertant mutations.

RT-PCR and RT-qPCR

RNA was isolated with the RNeasy mini kit (Qiagen) and was treated on-column with the RQ1 RNase-free DNase (Promega) and used for cDNA synthesis with the iScript cDNA synthesis kit (Bio-Rad). For visualization of the *CYCA3;4* splice variants created by the EMS mutation, cDNA made from RNA extracted from *pkn2 ccs52a2-1* and Col-0 was used as a template for RT-PCR using *CYCA3;4* primers (Supplemental Table 3), and the resulting amplicons were separated on a 1% (w/v) agarose gel containing 0.01% (v/v) SYBRSafe (Invitrogen). RT-qPCR was performed using the SYBR green kit (Roche) with 100 nM primers and 0.125 μL of RT reaction product in a total volume of 5 μL per reaction. Reactions were run and analyzed on the LightCycler 480 (Roche) according to the manufacturer's instructions with the use of the following reference genes for normalization: *EMB2386*, *PAC1*, and *RPS26E*. For each reaction, three technical repeats and two to three biological repeats were performed. All primer sequences used for RT-qPCR are listed in Supplemental Table 3.

Immunostaining Experiment

Plants were grown vertically on full-strength Murashige and Skoog medium (supplemented with 20 g/L Suc, 0.1 g/L myo-inositol, 0.5 g/L MES, 10 g/L thiamine hydrochloride, 5 g/L pyridoxine, 5 g/L nicotinic acid, pH adjusted to 5.7 with 1 M KOH, and 10 g/L plant agar) for 9 d. Root tips were fixed for 45 min in 4% (w/v) paraformaldehyde in a solution of 1× PME (50 mM Pipes pH 6.9, 5 mM $MgSO_4$, 1 mM EGTA) and then washed three times for 5 min in 1× PME. Root apices were dissected on a glass slide and digested in a drop of enzyme mix (1% [w/v] cellulase, 0.5% [w/v] cytohelicase, 1% [w/v] pectolyase in PME) for 1 h at 37°C. After three washes with PME, root apices were squashed gently between the slide and a cover slip, and frozen in liquid nitrogen. Afterwards, the cover slip was removed and the slides were left to dry for 1 h at room temperature.

For immunostaining, each slide was incubated overnight at 4°C with 100 μL of rabbit polyclonal anti-GUS antibody (N-terminal, 5420, Molecular Probes, Invitrogen) diluted 1:200 in fresh blocking buffer (3% [w/v] BSA in 1× PBS). Slides were washed three times for 5 min in 1× PBS solution and then incubated for 3 h at room temperature in 100 μL blocking buffer containing Alexa 488-conjugated goat anti-rabbit secondary antibody (Molecular Probes, Invitrogen), diluted 1:200 in fresh blocking buffer. Finally, DNA was counterstained with 2 μg/mL 4′,6-diamidino-2-phenylindole for 30 min, after which slides were washed in 1× PBS and mounted in mounting medium. The microscope settings and exposure times were kept constant for each respective channel.

Phosphoproteomics

Protein Extraction and Phosphopeptide Enrichment

Total protein extraction was conducted on three biological replicates of ~50 pooled 14-DAS-old whole *CYCA3;4*^{OE} 11.2 × wild type and wild type × wild type F1 seedlings, as previously described by Vu et al. (2017). Phosphopeptides were enriched as previously described with minor modifications (Vu et al., 2017). A total of 100 μL of the resuspended peptides was incubated with 3 mg MagReSyn Ti-IMAC microspheres for 20 min at room temperature. The microspheres were washed once with wash solvent 1 (80% [v/v] acetonitrile [ACN], 1% [v/v] trifluoroacetic acid [TFA], 200 mM NaCl) and twice with wash solvent 2 (80% [v/v] ACN, 1% [v/v] TFA). The bound phosphopeptides were eluted three times with 80 μL of an elution solution (40% [v/v] ACN, 1% [v/v] NH_4OH, 2% [v/v] formic acid), immediately followed by acidification to pH≤ 3 using 100% formic acid. Prior to MS analysis, the samples were vacuum dried and redissolved in 50 μL of 2% (v/v) ACN and 0.1% (v/v) TFA, of which 10 μL was injected for liquid chromatography-tandem mass spectrometry (LC-MS/MS) analysis.

LC-MS/MS Analysis

Each sample was analyzed via LC-MS/MS on an Ultimate 3000 RSLC nano LC (Thermo Fisher Scientific) in-line connected to a Q Exactive mass spectrometer (Thermo Fisher Scientific). The peptides were first loaded on a trapping column (made in-house, 100-μm internal diameter × 20 mm, 5-μm beads C18 Reprosil-HD, Dr. Maisch). After flushing the trapping column, peptides were loaded in solvent A (0.1% [v/v] formic acid in water) on a reverse-phase column (made in-house, 75-μm internal diameter × 250 mm, 1.9-μm Reprosil-Pur-basic-C18-HD beads, Dr. Maisch, packed in the needle) and eluted by an increase in solvent B (0.1% [v/v] formic acid in ACN) using a linear gradient from 2% solvent B to 55% solvent B in 180 min, followed by a washing step with 99% solvent B, all at a constant flow rate of 300 nL/min. The mass spectrometer was operated in data-dependent, positive ionization mode, automatically switching between MS and MS/MS acquisition for the five most abundant peaks in a given MS spectrum. The source voltage was set at 4.1 kV and the capillary temperature at 275°C. One MS1 scan (m/z 400 to 2,000, automatic gain control target 3 × 10^6

ions, maximum ion injection time 80 ms), acquired at a resolution of 70,000 (at 200 m/z), was followed by up to five tandem MS scans (resolution of 17,500 at 200 m/z) of the most intense ions fulfilling predefined selection criteria (automatic gain control target 5×10^4 ions, maximum ion injection time 80 ms, isolation window 2 Da, fixed first mass 140 m/z, spectrum data type centroid, under-fill ratio 2%, intensity threshold 1.3×10^4, exclusion of unassigned, 1, 5 to 8 and > 8 positively charged precursors, peptide match preferred, exclude isotopes on, dynamic exclusion time 12 s). The higher-energy collisional dissociation collision energy was set to 25% normalized collision energy and the polydimethylcyclosiloxane background ion at 445.120025 Da was used for internal calibration (lock mass).

Database Searching

MS/MS spectra were searched against the Arabidopsis database downloaded from The Arabidopsis Information Resource with MaxQuant software (version 1.5.4.1), a program package allowing MS1-based label-free quantification acquired from Orbitrap instruments (Cox and Mann, 2008; Cox et al., 2014). Next, the 'Phospho(STY).txt' output file generated by the MaxQuant search was loaded into the Perseus data analysis software (version 1.5.5.3) available in the MaxQuant package. Proteins that were quantified in at least two out of three replicates from each crossed line were retained. Log2 phosphopeptide intensities were centered by subtracting the median. A two-sample *t* test with a P value cutoff of P<0.01 was performed to test for differences between the crossed lines. Additionally, phosphopeptides with three valid values in each crossed line and none in the other were also retained and designated "unique" for that condition. All MS proteomics data in this study have been deposited to the ProteomeXchange Consortium via the PRIDE partner repository (Vizcaíno et al., 2016) with the data set identifier PXD017905.

Immunoblot

For immunoblot analysis, seeds were sown on nylon meshes (Prosep) on half strength Murashige and Skoog medium supplemented with 2% (w/v) Sucsucrose. Approximately 5-mm root tips from 1-week-old plants were harvested for protein extraction. Fifty micrograms total protein extracts were separated by means of SDS-PAGE and subsequently subjected to immunoblotting. Protein blots were hybridized with anti-RBR1 (Agrisera; catalog no. AS11 1627; 1:2000 dilution in 3% [w/v] skim milk) and anti-Phospho-RB (Ser807/811; 1:1000 dilution in 5% [w/v] BSA; Cell Signaling Technology; catalog no. 8516T) antibodies according to the manufacturer's description. Protein levels were quantified from two biological repeats, using three different exposures obtained from each repeat, using ImageJ.

Statistical Analysis

Statistical analyses were done as indicated in the figure legends, using either two-sample *t* tests or the ANOVA Mixed Model procedure in the SAS Enterprise Guide 7 software with Tukey- or Dunnett-correction for multiple testing. Details for each experiment can be found in Supplemental Data Set 4.

Accession Numbers

Sequence data from this article can be found in the Arabidopsis Genome Initiative or GenBank/EMBL databases under the following accession numbers: *CCS52A1* (AT4G22910), *CCS52A2* (AT4G11920), *CYCA3;1* (AT5G43080), *CYCA3;2* (AT1G47210), *CYCA3;3* (AT1G47220), *CYCA3;4* (AT1G47230), *WOX5* (AT3G11260), *SPCH* (AT5G53210), *FAMA* (AT3G24140), *RBR1* (AT3G12280), *EMB2386* (AT1G02780), *PAC1* (AT3G22110), and *RPS26E* (AT3G56340).

All MS proteomics data in this study have been deposited to the ProteomeXchange Consortium via the PRIDE partner repository (Vizcaíno et al., 2016) with the data set identifier PXD017905.

Supplemental Data

Supplemental Figure 1. Additional characteristics of the *ccs52a2-1* and *pkn2 ccs52a2-1* mutants (supports Figure 1).

Supplemental Figure 2. Detail of the allele frequency of EMS-specific mutations in *pkn2 ccs52a2-1* (supports Figure 2).

Supplemental Figure 3. The *pkn2* EMS mutation in *CYCA3;4* causes two different splice variants to be expressed (supports Figure 2).

Supplemental Figure 4. Analysis of *CYCA3;4* T-DNA insertion mutants (supports Figure 2).

Supplemental Figure 5. CCS52A protein accumulation patterns in the root tip (supports Figure 3).

Supplemental Figure 6. The CYCA3;4-GFP fusion protein is stabilized upon treatment with the proteasome inhibitor MG-132 (supports Figure 3).

Supplemental Figure 7. Expression levels and phenotypes of *CYCA3;4^{OE}* lines (supports Figures 7 and 8).

Supplemental Figure 8. Expression levels of *CYCA3;4* and *CCS52A2* in hemizygous *CYCA3;4^{OE}* lines (supports Figure 8).

Supplemental Table 1. Detailed annotation of the SNPs found for *pkn2 ccs52a2-1* in the interval selected on chromosome 1 from 14 Mbp to 18 Mbp (supports Figure 2).

Supplemental Table 2. Number of nuclei showing a CYCA3;4-GUS signal throughout the cell cycle in root tips with and without functional CCS52A2 (supports Figure 6).

Supplemental Table 3. Primer sequences.

Supplemental Data Set 1. List of identified phosphosites from phosphoprofiling of Col-0 × Col-0 (wild type) and *CYCA3;4^{OE}* 11.2 × Col-0 (OE) seedlings (supports Figure 9).

Supplemental Data Set 2. List of phosphosites significantly deregulated (Student's *t* test, $P < 0.01$) in Col-0 × Col-0 (wild type) versus *CYCA3;4^{OE}* 11.2 × Col-0 (OE) seedlings (supports Figure 9).

Supplemental Data Set 3. List of "unique" deregulated phosphosites from phosphoprofiling of Col-0 × Col-0 (wild type) versus *CYCA3;4^{OE}* 11.2 × Col-0 (OE) seedlings (supports Figure 9).

Supplemental Data Set 4. Statistical analysis.

ACKNOWLEDGMENTS

The authors thank Annick Bleys for help in preparing the manuscript. This work was supported by the Research Foundation Flanders (grants G023616N and G007218N), by the Agency for Innovation by Science and Technology in Flanders (predoctoral fellowship to A.W.), and by the Research Foundation Flanders (postdoctoral fellowship to J.H.).

AUTHOR CONTRIBUTIONS

A.W., J.H., I.D.S., and L.D.V. conceived and designed the research; A.W., J.H., T.E., I.A., J.A.P.-G., T.Z., L.L., H.V.d.D., I.V., and B.v.d.C. performed the experiments; A.W., J.H., T.E., J.A.P.-G., I.D.S., and L.D.V. analyzed the

data; A.W. and L.D.V. wrote the article; all authors read, revised, and approved the article.

Received March 17, 2020; revised June 12, 2020; accepted July 10, 2020; published July 20, 2020.

REFERENCES

Alonso, J.M., et al. (2003). Genome-wide insertional mutagenesis of *Arabidopsis thaliana*. Science **301:** 653–657.

Baloban, M., Vanstraelen, M., Tarayre, S., Reuzeau, C., Cultrone, A., Mergaert, P., and Kondorosi, E. (2013). Complementary and dose-dependent action of AtCCS52A isoforms in endoreduplication and plant size control. New Phytol. **198:** 1049–1059.

Borghi, L., Gutzat, R., Fütterer, J., Laizet, Y., Hennig, L., and Gruissem, W. (2010). *Arabidopsis* RETINOBLASTOMA-RELATED is required for stem cell maintenance, cell differentiation, and lateral organ production. Plant Cell **22:** 1792–1811.

Boudolf, V., et al. (2009). CDKB1;1 forms a functional complex with CYCA2;3 to suppress endocycle onset. Plant Physiol. **150:** 1482–1493.

Bouyer, D., Heese, M., Chen, P., Harashima, H., Roudier, F., Grüttner, C., and Schnittger, A. (2018). Genome-wide identification of RETINOBLASTOMA RELATED 1 binding sites in *Arabidopsis* reveals novel DNA damage regulators. PLoS Genet. **14:** e1007797.

Bulankova, P., Akimcheva, S., Fellner, N., and Riha, K. (2013). Identification of *Arabidopsis* meiotic cyclins reveals functional diversification among plant cyclin genes. PLoS Genet. **9:** e1003508.

Burke, J.R., Deshong, A.J., Pelton, J.G., and Rubin, S.M. (2010). Phosphorylation-induced conformational changes in the retinoblastoma protein inhibit E2F transactivation domain binding. J. Biol. Chem. **285:** 16286–16293.

Burke, J.R., Hura, G.L., and Rubin, S.M. (2012). Structures of inactive retinoblastoma protein reveal multiple mechanisms for cell cycle control. Genes Dev. **26:** 1156–1166.

Burke, J.R., Liban, T.J., Restrepo, T., Lee, H.-W., and Rubin, S.M. (2014). Multiple mechanisms for E2F binding inhibition by phosphorylation of the retinoblastoma protein C-terminal domain. J. Mol. Biol. **426:** 245–255.

Capron, A., Okrész, L., and Genschik, P. (2003). First glance at the plant APC/C, a highly conserved ubiquitin-protein ligase. Trends Plant Sci. **8:** 83–89.

Cebolla, A., Vinardell, J.M., Kiss, E., Oláh, B., Roudier, F., Kondorosi, A., and Kondorosi, E. (1999). The mitotic inhibitor ccs52 is required for endoreduplication and ploidy-dependent cell enlargement in plants. EMBO J. **18:** 4476–4484.

Clough, S.J., and Bent, A.F. (1998). Floral dip: A simplified method for *Agrobacterium*-mediated transformation of *Arabidopsis thaliana*. Plant J. **16:** 735–743.

Cools, T., Iantcheva, A., Maes, S., Van den Daele, H., and De Veylder, L. (2010). A replication stress-induced synchronization method for *Arabidopsis thaliana* root meristems. Plant J **64:** 705–714.

Cox, J., Hein, M.Y., Luber, C.A., Paron, I., Nagaraj, N., and Mann, M. (2014). Accurate proteome-wide label-free quantification by delayed normalization and maximal peptide ratio extraction, termed MaxLFQ. Mol. Cell. Proteomics **13:** 2513–2526.

Cox, J., and Mann, M. (2008). MaxQuant enables high peptide identification rates, individualized p.p.b.-range mass accuracies and proteome-wide protein quantification. Nat. Biotechnol. **26:** 1367–1372.

Cruz-Ramírez, A., et al. (2012). A bistable circuit involving SCARECROW-RETINOBLASTOMA integrates cues to inform asymmetric stem cell division. Cell **150:** 1002–1015.

da Fonseca, P.C.A., Kong, E.H., Zhang, Z., Schreiber, A., Williams, M.A., Morris, E.P., and Barford, D. (2011). Structures of APC/C^{Cdh1} with substrates identify Cdh1 and Apc10 as the D-box co-receptor. Nature **470:** 274–278.

De Veylder, L., Beeckman, T., and Inzé, D. (2007). The ins and outs of the plant cell cycle. Nat. Rev. Mol. Cell Biol. **8:** 655–665.

Dewitte, W., Riou-Khamlichi, C., Scofield, S., Healy, J.M.S., Jacqmard, A., Kilby, N.J., and Murray, J.A.H. (2003). Altered cell cycle distribution, hyperplasia, and inhibited differentiation in Arabidopsis caused by the D-type cyclin CYCD3. Plant Cell **15:** 79–92.

Facette, M.R., Rasmussen, C.G., and Van Norman, J.M. (2019). A plane choice: Coordinating timing and orientation of cell division during plant development. Curr. Opin. Plant Biol. **47:** 47–55.

Fülöp, K., Tarayre, S., Kelemen, Z., Horváth, G., Kevei, Z., Nikovics, K., Bakó, L., Brown, S., Kondorosi, A., and Kondorosi, E. (2005). *Arabidopsis* anaphase-promoting complexes: multiple activators and wide range of substrates might keep APC perpetually busy. Cell Cycle **4:** 1084–1092.

Gu, F., Bringmann, M., Combs, J.R., Yang, J., Bergmann, D.C., and Nielsen, E. (2016). Arabidopsis CSLD5 functions in cell plate formation in a cell cycle-dependent manner. Plant Cell **28:** 1722–1737.

Harashima, H., and Sugimoto, K. (2016). Integration of developmental and environmental signals into cell proliferation and differentiation through RETINOBLASTOMA-RELATED 1. Curr. Opin. Plant Biol. **29:** 95–103.

Heyman, J., Cools, T., Canher, B., Shavialenka, S., Traas, J., Vercauteren, I., Van den Daele, H., Persiau, G., De Jaeger, G., Sugimoto, K., and De Veylder, L. (2016). The heterodimeric transcription factor complex ERF115-PAT1 grants regeneration competence. Nat. Plants **2:** 16165.

Heyman, J., Cools, T., Vandenbussche, F., Heyndrickx, K.S., Van Leene, J., Vercauteren, I., Vanderauwera, S., Vandepoele, K., De Jaeger, G., Van Der Straeten, D., and De Veylder, L. (2013). ERF115 controls root quiescent center cell division and stem cell replenishment. Science **342:** 860–863.

Heyman, J., and De Veylder, L. (2012). The anaphase-promoting complex/cyclosome in control of plant development. Mol. Plant **5:** 1182–1194.

Heyman, J., Polyn, S., Eekhout, T., and De Veylder, L. (2017). Tissue-specific control of the endocycle by the Anaphase Promoting Complex/Cyclosome inhibitors UVI4 and DEL1. Plant Physiol. **175:** 303–313.

Karimi, M., Bleys, A., Vanderhaeghen, R., and Hilson, P. (2007). Building blocks for plant gene assembly. Plant Physiol. **145:** 1183–1191.

Karimi, M., Inzé, D., and Depicker, A. (2002). GATEWAY vectors for *Agrobacterium*-mediated plant transformation. Trends Plant Sci. **7:** 193–195.

Kevei, Z., Baloban, M., Da Ines, O., Tiricz, H., Kroll, A., Regulski, K., Mergaert, P., and Kondorosi, E. (2011). Conserved CDC20 cell cycle functions are carried out by two of the five isoforms in *Arabidopsis thaliana*. PLoS One **6:** e20618.

Lammens, T., Boudolf, V., Kheibarshekan, L., Zalmas, L.P., Gaamouche, T., Maes, S., Vanstraelen, M., Kondorosi, E., La Thangue, N.B., Govaerts, W., Inzé, D., and De Veylder, L. (2008). Atypical E2F activity restrains APC/C^{CCS52A2} function obligatory for endocycle onset. Proc. Natl. Acad. Sci. USA **105:** 14721–14726.

Larson-Rabin, Z., Li, Z., Masson, P.H., and Day, C.D. (2009). *FZR2/CCS52A1* expression is a determinant of endoreduplication and cell expansion in Arabidopsis. Plant Physiol. **149:** 874–884.

Lin, Q., et al. (2012). Rice APC/C(^{TE}) controls tillering by mediating the degradation of MONOCULM 1. Nat. Commun. **3:** 752.

Lin, Q., Wu, F., Sheng, P., Zhang, Z., Zhang, X., Guo, X., Wang, J., Cheng, Z., Wang, J., Wang, H., and Wan, J. (2015). The SnRK2-APC/C(TE) regulatory module mediates the antagonistic action of gibberellic acid and abscisic acid pathways. Nat. Commun. **6:** 7981.

Lin, Q., et al. (2020). The APC/C^{TE} E3 ubiquitin ligase complex mediates the antagonistic regulation of root growth and tillering by ABA and GA. Plant Cell **32:** 1973–1987.

Liu, Y., Ye, W., Li, B., Zhou, X., Cui, Y., Running, M.P., and Liu, K. (2012). CCS52A2/FZR1, a cell cycle regulator, is an essential factor for shoot apical meristem maintenance in *Arabidopsis thaliana*. BMC Plant Biol. **12:** 135.

Magyar, Z., Horváth, B., Khan, S., Mohammed, B., Henriques, R., De Veylder, L., Bakó, L., Scheres, B., and Bögre, L. (2012). *Arabidopsis* E2FA stimulates proliferation and endocycle separately through RBR-bound and RBR-free complexes. EMBO J. **31:** 1480–1493.

Marrocco, K., Bergdoll, M., Achard, P., Criqui, M.-C., and Genschik, P. (2010). Selective proteolysis sets the tempo of the cell cycle. Curr. Opin. Plant Biol. **13:** 631–639.

Mathieu-Rivet, E., Gévaudant, F., Sicard, A., Salar, S., Do, P.T., Mouras, A., Fernie, A.R., Gibon, Y., Rothan, C., Chevalier, C., and Hernould, M. (2010). Functional analysis of the anaphase promoting complex activator CCS52A highlights the crucial role of endo-reduplication for fruit growth in tomato. Plant J. **62:** 727–741.

Matos, J.L., Lau, O.S., Hachez, C., Cruz-Ramírez, A., Scheres, B., and Bergmann, D.C. (2014). Irreversible fate commitment in the *Arabidopsis* stomatal lineage requires a FAMA and RETINOBLASTOMA-RELATED module. eLife **3:** e03271.

Ossowski, S., Schneeberger, K., Clark, R.M., Lanz, C., Warthmann, N., and Weigel, D. (2008). Sequencing of natural strains of *Arabidopsis thaliana* with short reads. Genome Res. **18:** 2024–2033.

Page, A.M., and Hieter, P. (1999). The anaphase-promoting complex: New subunits and regulators. Annu. Rev. Biochem. **68:** 583–609.

Pfleger, C.M., and Kirschner, M.W. (2000). The KEN box: An APC recognition signal distinct from the D box targeted by Cdh1. Genes Dev. **14:** 655–665.

Polyn, S., Willems, A., and De Veylder, L. (2015). Cell cycle entry, maintenance, and exit during plant development. Curr. Opin. Plant Biol. **23:** 1–7.

Rasmussen, C.G., and Bellinger, M. (2018). An overview of plant division-plane orientation. New Phytol. **219:** 505–512.

Ren, S., and Rollins, B.J. (2004). Cyclin C/cdk3 promotes Rb-dependent G0 exit. Cell **117:** 239–251.

Shimada, T.L., Shimada, T., and Hara-Nishimura, I. (2010). A rapid and non-destructive screenable marker, FAST, for identifying transformed seeds of *Arabidopsis thaliana*. Plant J. **61:** 519–528.

Shimotohno, A., and Scheres, B. (2019). Topology of regulatory networks that guide plant meristem activity: Similarities and differences. Curr. Opin. Plant Biol. **51:** 74–80.

Su'udi, M., Cha, J.-Y., Jung, M.H., Ermawati, N., Han, C.D., Kim, M.G., Woo, Y.-M., and Son, D. (2012). Potential role of the rice *OsCCS52A* gene in endoreduplication. Planta **235:** 387–397.

Sun, H., and Schneeberger, K. (2015). SHOREmap v3.0: Fast and accurate identification of causal mutations from forward genetic screens. Methods Mol. Biol. **1284:** 381–395.

Takahashi, I., Kojima, S., Sakaguchi, N., Umeda-Hara, C., and Umeda, M. (2010). Two *Arabidopsis* cyclin A3s possess G1 cyclin-like features. Plant Cell Rep. **29:** 307–315.

Tarayre, S., Vinardell, J.M., Cebolla, A., Kondorosi, A., and Kondorosi, E. (2004). Two classes of the CDh1-type activators of the anaphase-promoting complex in plants: Novel functional domains and distinct regulation. Plant Cell **16:** 422–434.

Van Leene, J., et al. (2010). Targeted interactomics reveals a complex core cell cycle machinery in *Arabidopsis thaliana*. Mol. Syst. Biol. **6:** 397.

Vanstraelen, M., Baloban, M., Da Ines, O., Cultrone, A., Lammens, T., Boudolf, V., Brown, S.C., De Veylder, L., Mergaert, P., and Kondorosi, E. (2009). APC/C-^{CCS52A} complexes control meristem maintenance in the *Arabidopsis* root. Proc. Natl. Acad. Sci. USA **106:** 11806–11811.

Vizcaíno, J.A., et al. (2016). 2016 update of the PRIDE database and its related tools. Nucleic Acids Res. **44** (D1): D447–D456.

Vu, L.D., Verstraeten, I., Stes, E., Van Bel, M., Coppens, F., Gevaert, K., and De Smet, I. (2017). Proteome profiling of wheat shoots from different cultivars. Front Plant Sci **8:** 332.

Weimer, A.K., Nowack, M.K., Bouyer, D., Zhao, X., Harashima, H., Naseer, S., De Winter, F., Dissmeyer, N., Geldner, N., and Schnittger, A. (2012). Retinoblastoma related1 regulates asymmetric cell divisions in *Arabidopsis*. Plant Cell **24:** 4083–4095.

Wildwater, M., Campilho, A., Perez-Perez, J.M., Heidstra, R., Blilou, I., Korthout, H., Chatterjee, J., Mariconti, L., Gruissem, W., and Scheres, B. (2005). The *RETINOBLASTOMA-RELATED* gene regulates stem cell maintenance in *Arabidopsis* roots. Cell **123:** 1337–1349.

Xu, C., Wang, Y., Yu, Y., Duan, J., Liao, Z., Xiong, G., Meng, X., Liu, G., Qian, Q., and Li, J. (2012). Degradation of MONOCULM 1 by APC/C(^{TAD1}) regulates rice tillering. Nat. Commun. **3:** 750.

Yang, W., Wightman, R., and Meyerowitz, E.M. (2017). Cell cycle control by nuclear sequestration of *CDC20* and *CDH1* mRNA in plant stem cells. Mol. Cell **68:** 1108–1119.e3.

Yu, Y., Steinmetz, A., Meyer, D., Brown, S., and Shen, W.-H. (2003). The tobacco A-type cyclin, *Nicta;CYCA3;2*, at the nexus of cell division and differentiation. Plant Cell **15:** 2763–2777.